LBL-28819
UC-403

Lawrence Berkeley Laboratory
UNIVERSITY OF CALIFORNIA

EARTH SCIENCES DIVISION

Preliminary Studies of Gas Phase Flow Effects and Moisture Migration at Yucca Mountain, Nevada

Y.W. Tsang and K. Pruess

September 1989

LOAN COPY
Circulates
for 2 weeks
Bldg. 50 Library.
LBL-28819
Copy 2

Prepared for the U.S. Department of Energy under Contract Number DE-AC03-76SF00098.

DISCLAIMER

This document was prepared as an account of work sponsored by the United States Government. While this document is believed to contain correct information, neither the United States Government nor any agency thereof, nor the Regents of the University of California, nor any of their employees, makes any warranty, express or implied, or assumes any legal responsibility for the accuracy, completeness, or usefulness of any information, apparatus, product, or process disclosed, or represents that its use would not infringe privately owned rights. Reference herein to any specific commercial product, process, or service by its trade name, trademark, manufacturer, or otherwise, does not necessarily constitute or imply its endorsement, recommendation, or favoring by the United States Government or any agency thereof, or the Regents of the University of California. The views and opinions of authors expressed herein do not necessarily state or reflect those of the United States Government or any agency thereof or the Regents of the University of California.

LBL-28819

Preliminary Studies of Gas Phase Flow Effects and Moisture Migration at Yucca Mountain, Nevada

Y. W. Tsang and K. Pruess

Earth Sciences Division
Lawrence Berkeley Laboratory
University of California
Berkeley, California 94720

September 1989

This work was carried out under U.S. Department of Energy Contract No. DE-AC03-76SF00098, administered by the DOE Nevada Office, in cooperation with Sandia National Laboratories, Albuquerque.

Preliminary Studies of Gas Phase Flow Effects and Moisture Migration at Yucca Mountain, Nevada

Y. W. Tsang and K. Pruess

Earth Sciences Division
Lawrence Berkeley Laboratory
University of California
Berkeley, California

INTRODUCTION

The Yucca Mountain project is investigation the feasibility of siting a repository for high-level nuclear wastes at Yucca Mountain. Part of these investigations include estimates of the release of radionuclides to the accessible environment. Most of the radionuclides of interest will be transported in groundwater but a few radionuclides such as C^{14} could be transmitted through gaseous pathways (Von Konynenburg et al., 1985, 1986; Ross, 1987). An understanding of gas phase flow effects is necessary for determining the quantity of gaseous radionuclides such as C^{14} that could be released at the surface.

Gas phase flow has other ramifications besides providing potential pathways for radionuclides to the accessible environment. A study of thermal buoyancy flow induced by the heat load of a high-level nuclear waste repository has indicated that gas convection may take place with velocities of the order of 10 to 100 m/yr (Tsang and Pruess, 1987). This effect provides interesting possibilities for non-intrusive monitoring of repository performance. Furthermore, through vaporization and condensation processes coupled with vapor transport, gas phase flow effects may indirectly influence the distribution of moisture and liquid phase flow throughout the unsaturated zone.

Of paramount importance for an analysis of these coupled gas and liquid flow effects are the boundary conditions at the land surface. One can foresee that a number of factors at the boundary may play a role, either directly or indirectly, in affecting the gas movement and liquid infiltration in the mountain. These factors include: (1) gas

barometric pressure, (2) temperature, (3) precipitation, (4) wind velocity, (5) relative humidity of the atmospheric air, and (6) topography of the mountain.

The purpose of this work is to consider and understand the possible physical processes involving the physical parameters listed above, and to make simple estimates of the magnitude of these processes. We shall focus primarily on barometric pressure and relative humidity effects. A summary and discussion of precipitation and infiltration was given by Montazer and Wilson (1984). Topographic effects on gas flow have been studied by Weeks (1987) and Kipp (1987). The exercise of sorting out the relative importance of various competing processes is rather necessary. It will aid us in defining the appropriate boundary conditions to be used in subsequent full-scale simulations to model the gas flow at Yucca Mountain both at ambient conditions and with the repository heat load.

EFFECT OF BOUNDARY CONDITIONS ON GAS AND MOISTURE MOVEMENT

Effects of a relative humidity boundary condition

In this section we consider the role of a lowered humidity condition near the ground surface on the movement of moisture. Numerous mechanisms may carry moisture away from the land surface; these are evapotranspiration processes that are dependent on factors near the land surface such as temperature, hours of sunlight, wind velocity, the relative humidity of atmospheric air, temporal variations in availability of water at the surface, vegetation cover, and others (Brutsaert, 1982). As a result of the evapotranspiration, the humidity of the soil gas may be considerably lower near the land surface than at greater depth where we expect equilibrium with the liquid phase and close to 100% humidity. The lower relative humidity of the soil gas may be imposed as a boundary condition at the land surface, providing a driving force for the upward movement of moisture in the form of both liquid and vapor. In the following, we estimate the upward fluxes in response to the imposed boundary condition. An implicit assumption in this calculation is that any moisture flux brought up to the surface is carried away by the evapotranspiration process. Our results will show that this condition is definitely met.

There are several possible mechanisms by which the relative humidity of formation gas near the land surface may be reduced below 100%. The formations may be rather dry near the surface, so that the humidity level would reflect some kind of mixing between saturated soil gas at greater depth, and atmospheric air of low humidity. If capillary effects provide for the presence of soil moisture all the way up to the ground surface, a reduced humidity level can come about because of vapor pressure lowering. In the presence of capillary suction, vapor pressure is reduced from its saturated value according to Kelvin's equation (Edlefsen and Anderson, 1943):

$$P_v(T,S_l) = P_{sat}(T)\exp\left[\frac{P_{cap}(S_l)}{\rho_l RT}\right], \tag{1}$$

where ρ_l is the mass density of the water and R is the gas constant for water vapor: $8.314/18.016\times10^{-3}$ Joules/kg K. The relative humidity is defined as $h = P_v/P_{sat}$, so that

$$h = \frac{P_v}{P_{sat}(T)} = \exp\left[\frac{P_{cap}(S_l)}{\rho_l RT}\right]. \tag{2}$$

Another possibility for reduced humidity arises from non-equilibrium vaporization effects (Bixler, 1984). Barometric pressure variations will cause dryer atmospheric air to penetrate the ground surface and mix with ambient soil gas. If this mixing process occurs more rapidly than vaporization of soil moisture then vapor pressure will be reduced below the saturated value even with plenty of liquid water in the formation and weak vapor pressure lowering effects.

At Yucca Mountain it appears that because of the very small pore sizes of the tuffs the capillary effects are strong, so that the capillary fringe extends all the way to the ground surface. The reduced humidity level near the ground surface will cause an upward diffusive flux of vapor. If one assumes that the reduced vapor pressure is caused by vapor pressure lowering due to capillary suction, an additional upward flux of water will occur in the liquid phase. From the definition of Equation (2), the equivalent capillary suction as a result of the lower relative humidity boundary condition may be expressed as follows:

$$P_{cap}(S_l) = (\ln h)\,\rho_l RT. \tag{3}$$

The equivalent suction pressure may be quite strong even with moderate lowering of humidity level as indicated in Table 1, where some representative values of P_{cap} as

function of humidity, h, at the temperature of 286 K are given. The strong suction pressure provides a driving force for an upward movement of liquid water toward the low humidity boundary, given by:

$$\mathbf{F}_l = -\bar{k}\,\frac{k_{rl}}{\mu_l}\rho_l\,(\nabla\,(P_g + P_{cap}) - \rho_l\,\mathbf{g}), \tag{4}$$

where $\bar{k}$ is the saturated permeability of the fractured porous medium, k_{rl} is the relative permeability to the liquid phase at the liquid saturation S_l, μ_l is the viscosity of the liquid, P_g is the gas pressure, $\mathbf{g}$ is the gravitational acceleration, and $\mathbf{F}_l$ is the liquid mass flux. If reduced humidity in the formation gas beneath the land surface is attributed to non-equilibrium vaporization rather than vapor pressure lowering effects, then the liquid flux will be less than that given by Equation (4).

The lower humidity boundary condition also implies a composition gradient in the gas phase, giving rise to a downward flux of air and an equal upward flux of vapor by means of binary diffusion. The binary diffusion gas flux is described by:

$$\mathbf{F}^{\kappa} = -D_{va}\,\rho_g\,\nabla\chi_g^{\kappa}, \tag{5}$$

where κ is the component index for the gas phase (κ=air or vapor), χ_g^{κ} is the mass fraction of the κth component in the gas phase and D_{va} is the diffusion coefficient for the vapor-air mixture given by (Vargaftik, 1975; Walker et al., 1981),

$$D_{va} = \tau\phi S_g D_{va}^{o}\,\frac{P_o}{P}\,(\frac{T}{T_o})^{\theta}\,. \tag{6}$$

Here, ϕ is the porosity, S_g is the gas saturation, τ is a tortuosity factor, which is dependent on the pore geometry, T is the temperature in degrees Kelvin, D_{va}^{o} is the diffusivity at reference conditions of $T_o = 273.15$ K and $P_o = 1$ bar and θ is 2.334.

The above discussion shows that the humidity boundary condition provides a driving force for upward flux of water in both phases. To estimate the magnitude of these fluxes, calculations were carried out by means of the numerical simulator "TOUGH" (transport of unsaturated groundwater and heat) developed by Pruess (1987). To focus on the vertical movement of water, the simulation was carried out in one dimension, in a vertical tuff column of height 600 m, which is the approximate distance of the land surface to the water table (see Figure 1). Although the geology of Yucca Mountain consists of alternating layers of welded and non-welded tuff units,

each unit with different formation and hydrological characteristics, we employ here a highly simplified stratigraphic description, assuming constant hydrological parameters throughout. These parameters were chosen to be representative of the potential repository host formation (the Topopah Spring welded unit). A summary of all material properties and characteristic curves for the matrix and fracture is given in Table 2, which is identical to that used previously (Tsang and Pruess, 1987; Pruess et al., 1988) in a study of thermally induced convection near a high-level nuclear waste repository in tuff. A comparison of the data used in this report with data in RIB is given in Appendix B. In our computations we also utilize the "effective continuum" approximation (Pruess et al., 1985, 1988). In this approximation the fractured porous medium is treated as one effective continuum characterized by effective parameters. The fractures are not modeled explicitly, but their effects are represented by means of appropriate gas and liquid effective (relative) permeabilities. The effective continuum parameters are defined in terms of matrix and fracture parameters. A discussion of the definition of the characteristic curves in the effective continuum approximation is presented in Appendix A. Figure 2 plots the effective continuum liquid permeability and the capillary suction pressure as a function of the effective continuum liquid saturation S_l. For the parameter values used, the fracture is drained of liquid for S_l below .9839; therefore the characteristic curves in Figure 2 represent that of the rock matrix for a large range of S_l. Note that the suction pressure and the permeability are both in logarithmic scale and the relative permeability drops by several orders of magnitude as the continuum liquid saturation decreases.

The numerical computation is carried out in two steps. First, we simulate the one-dimensional vertical column between water table and ground surface with all problem specifications of Table 2 in place. The ground surface and the water table are constant temperature boundaries maintained at 286 K and 304 K, respectively. Moreover, the water table also serves as a constant pressure boundary of 1 bar with the effective continuum liquid saturation of 1 and zero capillary suction. By this we obtain as a function of elevation the equilibrium profiles of temperature, gas pressure, vapor pressure, and liquid and gas saturations at ambient conditions before the boundary condition of lower humidity at the land surface is engaged. In the second step of the computation, we impose, in addition to the boundary conditions in step 1, the equilibrium ambient gas pressure at the land surface as well as an additional liquid suction pressure

corresponding to Equation (3) at the surface node to implement the lower humidity boundary condition. Calculations were carried out for two values of humidity: (1) h=0.8, and (2) h=0.5. The results of our investigations are presented in Figures 3 through 10.

In Figures 3 through 10 we label the results simulated for ambient conditions prior to imposition of reduced humidity boundary condition "reference case"; the simulated results with imposed humidity boundary conditions are labeled "80% humidity" and "50% humidity." Figure 3 shows the temperature profiles for ambient conditions and for 50% humidity boundary conditions. The two profiles are very similar; the slightly higher temperatures for the calculations with 50% humidity boundary condition perhaps arise from the the upward liquid flux which brings up warmer liquid from the water table. The profile for the calculations with 80% humidity boundary condition is almost identical to that of the 50% humidity boundary condition and is therefore not displayed in the figure. Figure 4 gives the equilibrium gas pressure profile prior to imposition of reduced humidity boundary conditions. Recall that the gas pressures at the top and bottom of the column were kept fixed for all the simulations with reduced humidity boundary conditions. Figure 5 and Figure 6 show, respectively, the equilibrium vapor pressure and the equilibrium humidity of the soil gas within the tuff formation. Note that the vapor pressure and the relative humidity profiles deviate from the ambient only in the upper 150 m of the column. Figures 7 and 8 show the profiles of equilibrium liquid saturation and the capillary suction pressure. Note that because of the very strong capillary pressures the capillary fringe extends all the way to the ground surface. Figure 7 shows that as a result of the upward movement of moisture and its subsequent loss at the land surface, the liquid saturation profiles shift quite dramatically to lower values for the lower humidity boundary conditions. Figure 8 shows the very strong capillary suction in the top half of the tuff column corresponding to the smaller liquid saturations.

Figure 9 shows the mass fraction of air in the gas phase, the gradient of which is the driving force for the upward flux of vapor by binary diffusion. It is clear from Figure 9 that in the top 150 m of the column, the gradient and therefore the vapor flux due to binary diffusion is increased, with respect to the values of the reference case, by perhaps a factor of 2 with the 80% humidity boundary, and a factor of 3 to 4 with the 50% boundary condition. At ambient conditions of the reference case the upward

vapor flux due to binary diffusion arises from the decrease of vapor pressure with elevation because of the thermal gradient. Without the lowered humidity boundary conditions at the surface, the upward movement of the moisture in the gas phase is exactly balanced by a downward movement of the liquid phase. Ross (1984) has estimated the magnitude of binary diffusion vapor flux under ambient conditions in a deep unsaturated zone, taking into account that the vapor pressure varies only with the geothermal temperature gradient. He arrived at an upward vapor flux which is equivalent to .03 mm/yr of water. Our simulations give values ranging from .04 mm/yr at depth to .015 mm/yr at the land surface for $\mathbf{F}^v/\tau\phi S_g$ as defined in Equations (5) and (6) at ambient conditions. For the prevailing liquid saturation of the tuff column at equilibrium, the fractures are essentially drained of liquid, so the gas phase flow occurs predominantly in the fractures, characterized by the parameters $S_g = 1$, $\tau = 1$, and $\phi_f = .0018$ (Table 2). With these parameter values, the binary diffusion vapor flux $\mathbf{F}^v$ will be equivalent to liquid flux of the order of only .00007 mm/yr at ambient, and .0002 mm/yr with reduced humidity boundary conditions. In Ross's (1984) estimation, the factor $(\tau S_g \phi)$ takes on an equivalent value of about 2.

While the liquid flux is downward to balance the upward vapor flux by binary diffusion in the ambient case, both the gas and liquid fluxes are upward with the lower humidity boundary conditions. Figure 10 gives the magnitude of the upward liquid Darcy velocities for the two lower humidity boundary conditions. It is interesting to note that the liquid velocity is essentially constant from the water table (elevation 0 m) to within 150 m of the surface and then sharply decreases (note the logarithmic scale). This can be explained as follows. The lower humidity boundary condition translates to very strong suction at the boundary (Equation (3)), giving rise to very large pressure gradient (Figure 8) as the driving force for the liquid flux (Equation (4)), however, at the lower liquid saturation near the surface, the liquid relative permeability drops by several orders of magnitude (Figure 2a) which diminishes the liquid flux despite the large pressure gradient. In fact, the 50% humidity boundary with a more negative capillary suction actually gives rise to smaller upward liquid fluxes in the top part of the tuff column, although at the water table, the 50% humidity boundary condition indeed gives rise to a slightly larger upward liquid flux. It should be pointed out that the steep drop in the relative permeability with decreasing liquid saturation shown in Figure 2 describes the behavior of liquid movement in the matrix. However, at present

it is not known whether liquid could be mobile on the walls of the drained fractures. In that case liquid relative permeability would not drop off as rapidly with saturation, and significantly larger fluxes could occur.

The above results indicate that given the characteristic curves of the Topopah Spring welded tuff unit used here, the magnitudes of the upward liquid and vapor fluxes as a result of relative humidity boundary conditions are small, on the order of .001 mm/yr and .0002 mm/yr respectively. These values are several orders of magnitudes smaller than the annual precipitation at Yucca Mountain which is estimated to range from 100 to 150 mm (Montazer and Wilson, 1984). They are even more negligibly small with respect to the potential evapotranspiration which in this arid region is estimated to be five times that of the annual precipitation (Environment Assessment Report DOE/RW-0073, 1986, section 3.3.1)

Effects of atmospheric pressure variation

Moisture from the formation may be removed as a result of atmospheric pressure variations with time at the land surface; we shall denote this process by "barometric pumping." Assume an initial condition where the pressure of the gas phase in the formation immediately beneath the land surface is at equilibrium with the atmospheric pressure. As the atmospheric pressure increases, air with rather low relative humidity is forced into the soil. Its humidity then increases from mixing with soil gas and from evaporation of soil moisture. When atmospheric pressure decreases at a later time, this more humid soil gas is discharged back to the atmosphere. Because the incoming gas has a lower relative humidity than the outgoing gas, this "pumping" process, due to atmospheric pressure variations, provides a mechanism for loss of formation moisture.

To obtain an order of magnitude estimate of the moisture loss due to "barometric pumping," we may start with the ideal gas law

$$PV = nRT. \tag{7}$$

When the atmospheric pressure increases by a small amount ΔP, a volume V of formation gas is compressed by ΔV, where

$$(P+\Delta P)(V-\Delta V) = PV = PV + \Delta PV - \Delta VP - \Delta P\Delta V. \tag{8}$$

To first order in ΔP and ΔV for small variations of pressure and volume, Equation (8)

becomes

$$\frac{\Delta P}{P} = \frac{\Delta V}{V} = \frac{\Delta H}{H} \tag{9}$$

where H is the height of the gas column from the ground surface to the water table and ΔH is the decrease in height as a result of rising atmospheric gas pressure. The volume of atmospheric air entering the formation per unit cross-sectional area is $\Delta H \phi S_g$, where ϕ is the porosity of the formation and S_g is the gas saturation. We denote the mass fraction of vapor in atmospheric air by χ_{in}. When at some later time the atmospheric pressure drops again by ΔP, the same gas volume of $\Delta H \phi S_g$ is discharged to the atmosphere, but with an increased mass fraction χ_{out} of water vapor. The net mass of water removed as vapor from the formation per unit area during one pumping cycle (P to P+ΔP and back to P) is then

$$M = \Delta H \phi S_g \rho_g (\chi_{out} - \chi_{in}) = H(\Delta P/P) \phi S_g \rho_g (\chi_{out} - \chi_{in}). \tag{10}$$

If moist air is approximated as an ideal gas, the definition of relative humidity, Equation (2), can be rewritten as

$$h = \chi / \chi_{sat}, \tag{11}$$

where χ_{sat} is the saturated vapor mass fraction. Equation (10) then becomes

$$M = H(\Delta P/P) \phi S_g \rho_g \chi_{sat} (h_{out} - h_{in}). \tag{12}$$

The magnitude of $\Delta P/P$ and the relative humidity h_{in} will be deduced from the meteorological data. Sandia National Laboratories installed two 10-meter meteorological tower systems located at two sites near Yucca Mountain, one at site YA (Yucca Alluvial) in the valley to the east of Yucca Mountain, the other at site YR (Yucca Ridge) near the ridge top of Yucca mountain. Data collection covered the period from July 1982 through October 1984. The hourly data recorded on magnetic tape were made available to us by Hugh Church; the summary of the data are in the reports (Church et al., 1983, 1984, 1985, 1986). Because the idea of moisture removal by barometric pumping hinges on some kind of cyclical variation of the pressure, we performed a Fourier analysis of the hourly pressure data to uncover any periodicity in the variation. The hourly pressure data at the Ridge site are plotted in Figure 11. The horizontal axis covers the 2-year period from January 1, 1983 through December 31, 1984, with the 8761st hour corresponding to the first hour of January 1, 1983. Apart

from the pressure data, another plot is displayed immediately above the x axis. On this plot, the times for which pressure data are available are marked by a horizontal line, and time intervals in which data are missing are marked by gaps in the horizontal line bracketed by short vertical lines. It is clear from this plot in Figure 11 that the longest stretch of unbroken data on the Ridge site with little missed readings (there are a few 1- or 2- hour gaps and one 6-hour gap which, due to the shortness of interval, show up only as vertical tick marks on the horizontal line) occurs from August 1983 through October 1984. In this 15-month period, there are five segments of 2 to 3 month duration in which there is no missed reading at all. These segments are labeled A through E in Figure 11. Fourier analysis was done on each of the five segments using a Fast Fourier Transform Routine (C06EAF in NAG, Library of Mathematical Routines). The resultant power spectra for the five segments are shown in Figure 12. The y axis is the absolute value squared of the Fourier coefficients. It is clear that a periodicity of 24 hours is common to all the four segments of data. A weaker peak in the power spectra corresponding to a period of 12 hours is also observed for all the segments; this Fourier component is the first harmonic of the frequency corresponding to the period of 24 hours. Because the smallest period uncovered by the Fourier analyses done on the short stretches of unbroken data (segments A-E) is 12 hours, it seems safe now to analyze the entire stretch of data covering 15 months in Figure 11, treating the data as one continuous unbroken piece by linearly interpolating the missing data of typically 1 to 2 hours (with the exception of one 6-hour gap) which separate the segments A through E. The power spectrum is shown in Figure 13 where the y axis is in logarithmic scale. It is clear that all the apparent periodicities larger than 24 hours which appeared in Figure 12 when shorter stretches of data were analyzed are no longer present. The white noise of the spectrum indicates the stochastic nature of the pressure data other than the 24-hour period. We note the peaks in the power spectrum corresponding to the higher harmonics of the fundamental frequency, 1/24 hour^{-1}. These higher harmonic components may all contribute to the periodic variation of the pressure data in the time domain with the fundamental frequency, that is, that which corresponds to a period of 24 hours. Because of the noise level in the power spectrum from the fast Fourier Transform, we used the method of Spectral Analysis where a window is applied to smooth out the white noise in the frequency domain. We employ the routine G13CAF from the NAG Library of Mathematical Routines, using a Parzen

lag window, to arrive at the smoothed spectrum as shown in Figure 14. It is interesting to note that the stochastic part of the log-log power spectrum plot displays a linear slope with period, indicating that the amplitude of fluctuations in the pressure data increases with increasing "periods," which is characteristic of a fractal structure (Mandelbrot, 1983).

With the period of atmospheric data established, we would like to estimate the maximum change in pressure per cycle, that is, ΔP in Equation (12). Processing all the pressure data from 1982 through 1984, we find that the average ΔP in the 24-hour cycle is .5 kPa at the Ridge site, and .8 kPa at the Alluvial site. The mean pressure over the same period is 85.2 kPa.

A statistical analysis of the atmospheric relative humidity data over the period of 2 to 3 years gives the mean value of 0.28 for the Ridge site and 0.33 for the Alluvial site. We make the conservative assumption that the soil gas in the formation is very nearly saturated, and therefore has relative humidity of 1.0. This will give a maximum estimate for the amount of water that can be removed from the formation by barometric pumping. The other parameters in Equation (12) are chosen as follows:

$$H \approx 600\,\mathrm{m}$$

$$\Delta P \approx .5\,\mathrm{kPa} \text{ at Ridge site}$$

$$P \approx 85.2\,\mathrm{kPa}$$

$$\chi_{out} \approx 1.$$

$$\chi_{in} \approx .28 \text{ at Ridge site}$$

$$\phi \approx 0.1$$

$$S_g \approx 0.2$$

and the value $57.84\,\mathrm{m}^3/\mathrm{kg}$ for $1/\rho\chi_{sat}$ from the specific volume of saturated steam at 20°C as obtained from the Steam Tables (ASME Steam Tables). Inserting these numerical values into Equation (12), we obtain

$$\text{Mass of vapor removed/pressure cycle} = 8.77\mathrm{x}10^{-4}\,\mathrm{kg}.$$

Because the pressure cycle is 1 day, the net moisture removed from the formation per year per m^2 of surface area is $8.77 \times 10^{-4} \times 365 = 0.32\mathrm{kg}$. This will translate to about

.32 mm/yr of water. The pressure variation also has a periodicity of one year, with a larger amplitude of the order of 1 kPa, then ΔP is 2 kPa, a factor of 4 larger than the pressure variation with the 24 hour period; however, the number of cycles in 1 year is now reduced by a factor of 365. Therefore the amount of moisture that may be removed by the pressure variation with the 1-year period is almost two orders of magnitude smaller than that attained by the 24-hour cyclic variation. We conclude that the 24-hour cycle pressure variation is the dominant process in "pressure pumping" moisture out from the formation.

DISCUSSION

The simple calculations presented in the previous section show that the different processes considered involve only very small upward fluxes of the vapor component in the gas phase. The heat generation after the repository is loaded is expected to provide a much larger upward driving force through buoyancy effects (Tsang and Pruess, 1987) than the processes considered here for ambient conditions. We have shown in that calculation that buoyancy effects can account for velocity on the order of tens of meters per year, which can play a significant role in the advective transport of C^{14} in the gas phase flow.

Gas phase flow effects were found to make only a minor contribution to overall saturation distribution and infiltration balance throughout the mountain (less than 1 mm/yr, compared with the annual precipitation of approximately 150 mm/yr). This result needs to be qualified, however, because in our simplified estimations we did not take the layering of the tuff formations into account. We also did not allow for liquid mobility on the walls of drained fractures, which is a possibility that has not been ruled out experimentally.

Net liquid infiltration

Apart from the question of the possible upward movement of gaseous radionuclides, the upward vapor fluxes also induce an upward movement of moisture from the formation to the atmosphere. The effect of a lowered relative humidity for the soil gas at the boundary gives rise to a vapor flux corresponding to .0002 mm/yr of water; and the effect of periodic atmospheric pressure variation gives rise to a vapor flux which

we have estimated as equivalent to .32 mm/yr of water. The effects of seasonal variation of air temperature coupled with the topography of Yucca Mountain on the air circulation in the boreholes open to the unsaturated zone have been considered by Weeks (1987) and Kipp (1987). Kipp performed a numerical simulation of the air flow and estimated that the net water vapor transported out from the simulated region is equivalent to about .04 mm/yr. These upward vapor fluxes are several orders of magnitude smaller than the potential evapotranspiration expected in the region, which, because of the extreme aridity of the region, is expected to be about five times that of the annual precipitation of about 150 mm/yr (Environment Assessment Report DOE/RW-0073 section 3.3.1, 1986; Montazer and Wilson,1984; Quiring, 1983).

On the other hand, despite their small values, these upward fluxes are of the same order of magnitude as some recent estimates of net infiltration (Montazer and Wilson, 1984). With the presence of several competing processes of minute amounts of moisture moving in opposite directions, a natural question arises as to the possibility of a scenario of an overall drying of Yucca Mountain and receding of the water table. On the other hand, the upward moisture fluxes calculated here arise from an imposed boundary condition at the land surface, and it is known that in unsaturated zones that are hundreds of meter thick, the surface fluctuations in soil moisture that result from episodic infiltration followed by evapotranspiration become totally damped at depth, and deep percolation becomes nearly constant in time. Hence the relevant question is how these upward vapor fluxes arising from land surface boundary conditions affect the percolation fluxes at the repository level in the Topopah Spring member of the welded tuff. In order to evaluate the net effect of these competing processes of moisture movement, we shall review briefly here the methods which lead to the estimate that the net downward infiltration liquid flux is on the order of mm per year.

Estimates of downward liquid flux

A review of estimates of net liquid infiltration was recently made by Montazer and Wilson (1984). Estimates of recharge typically lie in the mm-per-year range. All methods to estimate the infiltration flux are indirect. One line of reasoning uses an estimate of the recharge through the unsaturated zone to the saturated zone. Direct measurement of the recharge has not been made at Yucca Mountain. An empirical method (Eakin et al., 1951) used extensively in Basin studies in Nevada relates the

recharge for ground water basins to total precipitation, with larger recharge percentages being assigned to larger precipitation. Rush (1970) applied the method to estimate recharge to ground water basins in Southern Nevada. Czarnecki (1984) used Rush's (1970) results and estimated recharge to be about 0.5-0.7 mm/yr in a precipitation zone that includes Yucca Mountain as well as parts of Jackass Flats and Crater Flat. The recharge to the carbonate aquifer underlying much of the Nevada Test Site and vicinity is estimated to be 3% of the precipitation (Winograd and Thordarson, 1975). Montazer and Wilson applied this percentage to the annual precipitation at Yucca Mountain (150 mm/yr) to obtain a recharge rate of about 4.5 mm/yr. Waddell et al. (1984), using data from Winograd (1981), estimated a flux of about 0.5 mm/yr through alluvium in Yucca Flat, about 40 km northeast of Yucca Mountain.

A second indirect method to estimate the liquid flux is through interpretation of thermal data. In this method, the linear segments of the formation temperature profiles are attributed to conductive heat flows, and the systematically non-linear segments displaying curvature in temperature-depth profile are attributed to convective flow. Sass and Lachenbruch (1982) analyzed data from 60 wells in and around Nevada Test Site, including 16 in the Yucca Mountain area. The thermal data of the drill holes indicate a thermal regime characterized by both vertical and lateral gradient in heat flow. The large variations of heat flow on both regional and local scale are attributable primarily to hydrologic processes involving interbasin flow. In particular, Sass and Lachenbruch interpreted a large area of anomalously low heat flow as reflecting regional flow with a downward component of seepage velocity. In interpreting the data of increasing heat flow with depth, Sass and Lachenbruch employed a one-dimensional diffusive vertical flow model (Lachenbruch and Sass, 1977; Bredehoeft et al., 1965) to estimate the vertical seepage velocity and arrived at the value of a few mm per year.

The third indirect method of estimating the vertical liquid flux in the unsaturated zone is by means of its effective hydraulic conductivity. In thick unsaturated zones, the fluctuating liquid saturation and matric potential (cf. capillary suction pressure) at the surface become damped out at depth, so that the liquid saturation and the matric potential become uniform with depth in the thick unsaturated zone away from the surface of the water table. In this region for a uniform porous medium, the total hydraulic head is unity due to gravity, and by Darcy's law the vertical flux is exactly equal to the

hydraulic conductivity at the prevailing liquid saturation.

Anderson (1981) performed laboratory permeability measurements, using water as the test fluid on 15 cores of the Topopah Spring member of the paintbrush tuff from test well UE25a#1. He arrived at a saturated hydraulic conductivity of the tuff matrix in the range of 4-7 $x10^{-11}$ m/s corresponding to 1.3-2.2 mm/yr. Weeks and Wilson (1984) performed laboratory analyses on the hydrologic properties of unsaturated tuff. They evaluated the relative conductivity of 19 cores collected at depths ranging from about 34 to 533 m from test well USW H-1, which is located at 2.0 km west of test well UE25a#1. Of the nineteen samples, one was from the Paintbrush non-welded unit, sixteen were from the Topopah Spring welded hydrologic unit, and two from the Calico Hills non-welded unit. The measured relative conductivity ranges from 0.002 to 0.1 in the range of the in situ ambient matrix saturations. Combining these results with those of Anderson (1981) on saturated conductivities, and assuming a hydraulic head gradient equal to unity, one arrives at the vertical downward flux to be in the range of .003 to 0.2 mm/yr.

The above estimates of downward flux from hydraulic conductivities of the core samples are based on the assumption that the hydraulic gradient is unity. The unsaturated zone at Yucca Mountain is not a uniform porous medium; rather it consist of alternating layers of welded and non-welded tuffs with different hydrologic properties. Therefore, different liquid saturation and matric potential profiles may occur in different layers and the notion of unit hydraulic head becomes fuzzy. The matric potential and liquid saturation within each layer away from the boundaries may be quite uniform so that the hydraulic conductivity may still be equated to the vertical flux; however, due to the sparseness of data and uncertainties in their reliability, the validity of the assumption of unit hydraulic head gradient cannot presently be verified. The downward flux estimated from this indirect method therefore carries with it an uncertainty.

It is clear from the above summary that at the present time, there is no definitive estimate of the vertical liquid flux in the unsaturated zone at Yucca Mountain. Of the three indirect methods for estimating the net vertical flux at depth, it seems that the last approach which makes use of the hydraulic conductivity has the potential of being the most "accurate." To remove the ambiguity of the unit hydraulic gradient

assumption, more complete data of matric potential, liquid saturation, and relative permeability are needed so that their profiles with depth may be compiled. This kind of measurement can lead to an answer as to the direction and magnitude of the vertical liquid flux at Yucca Mountain.

Experimental determination of actual evaporation

Not only are experimental data needed to answer the question of the magnitude of percolation liquid flux at depth; measurements to obtain the magnitude of moisture fluxes leaving the mountain may also be relevant. Our review of the literature on investigations at Yucca Mountain indicates that data of actual evaporation from Yucca Mountain do not exist. Because the potential evaporation rate may grossly overestimate the actual evaporation in very arid regions (Brutsaert, 1982), measurements of the actual evapotranspiration at Yucca Mountain may be important. Most of the measurements of evaporation involve either the direct application or some approximation of the energy budget equation. For practical purposes, a simplified form of the energy budget (for example, Brutsaert, 1982) is written as

$$L_eE + H = R_n \tag{13}$$

where R_n, the net flux density of radiation, is the main component of energy supply, balanced by losses of latent heat L_eE and sensible heat H into the atmosphere, with E being the rate of evaporation and L_e the latent heat of evaporation. If the Bowen ratio B_o is defined as

$$B_o = H/L_eE \ , \tag{14}$$

then Equation (13) may be rewritten as,

$$E = \frac{R_n/L_e}{1+B_o} \ . \tag{15}$$

At the present time, fairly reliable instruments are available for measuring the net radiation R_n (Brutsaert, 1982; Jackson et al., 1985). The Bowen ratio, B_o, may be obtained from profile data of relative humidity and temperature in the atmospheric surface sublayer (Brutsaert, 1982), so that the evaporation rate, E, can then be calculated from Eqution (15). This method, known as the energy budget Bowen ratio method, is widely used to estimate vertical flux density on a local scale. In cases where profile

data of the temperature or of the specific humidity are lacking, it is possible to use instead the mean wind-speed profile in the application of the energy budget method. This method has been applied by Sticker and Brutsaert (1978) to determine evapotranspiration from grass.

Direct measurements of evapotranspiration from the surface at Yucca Mountain can certainly reduce the uncertainty in the estimation of water infiltration at the mountain. It would seem that an experimental program to determine the evapotranspiration would be of considerable value to the Yucca Mountain Project.

SUMMARY

We have examined and reviewed the effect of atmospheric boundary conditions at the land surface on the ambient gas and moisture movements at Yucca Mountain. The Preliminary investigations were done by considering an one-dimensional column of tuff with the properties and characteristic curves of the Topopah Spring welded unit. In general, we find the magnitude of the fluxes for different processes considered here to be minute, on the order of 0.1 mm/yr. Vapor fluxes have comparable magnitude, but move in the opposite direction as the estimated net liquid infiltration. A rational model of water infiltration should be based on a realistic energy balance at the ground surface. This will require an adequate resolution of temporal variations of precipitation and other weather patterns. No rational evaporation-infiltration model has yet been developed for Yucca Mountain; at the present time, all estimates of the downward liquid flux in the partially saturated zone remain indirect and fraught with uncertainty. We strongly recommend an effort to experimentally determine the actual evapotranspiration from surface temperature and meteorological data, and to incorporate this into a rational model for the estimate of the liquid infiltration.

ACKNOWLEDGEMENT

Help from Frank Hale in the handling of the pressure weather data is very much appreciated. Review and comments from Andy Peterson and Roger Eaton of Sandia National Laboratories are gratefully acknowledged. This work was carried out under U. S. Department of Energy Contract No. DE-AC03-76SF00098, administered by DOE Nevada Office, in cooperation with the Sandia National Laboratories, Albuquerque.

REFERENCES

Anderson, L. A., Rock Property Analysis of Core Samples from the Yucca Mountain UE25A-1 Borehole, Nevada Test Site, Nevada, USGS open-file report 81-1338, 1981.

Bird, R. B., W. E. Stewart and E. N. Lightfoot, *Transport Phenomena,* J. Wiley and Sons, New York, NY, 1960, P.505.

Bixler, N. E., NORIA-a Finite Element Computer Program for Analyzing Water, Vapor, Air, and Energy Transport in Porous Media, SAND84-2057, Sandia Nat. Lab., Albuquerque, NM, 1984.

Bredehoeft, J. D., and Papadopulos, I. S., Rates of Vertical Ground Water Movement Estimated from the Earth's Thermal Profile, Water Resour. Res., 1, 325-328, 1965.

Brutsaert, W., *Evaporation into the Atmosphere, Theory, History, and Applications,* D. Reidel Publishing Company, Dordrecht, Holland, 1982.

Church, H. W., D. L. Freeman, K. Boro, R. T. Egami, Meteorological Tower Data for the Nevead Nuclear Waste Storage Investigations, SAND83-1912, Sandia Nat. Lab., Albuquerque, NM, 1983.

Church, H. W., D. L. Freeman, K. Boro, R. T. Egami, Meteorological Tower Data for the Neveda Nuclear Waste Storage Investigations, SAND84-1327, Sandia Nat. Lab., Albuquerque, NM, 1984.

Church, H. W., D. L. Freeman, K. Boro, R. T. Egami, Meteorological Tower Data Yucca Ridge (YR) Site, Jan-June, 1983, SAND85-1053, Sandia Nat. Lab., Albuquerque, NM, 1985.

Church, H. W., D. L. Freeman, K. Boro, R. T. Egami, Meteorological Tower Data for the Yucca Alluvial (YA) Site SAND86-2533, Sandia Nat. Lab., Albuquerque, NM, 1986.

Czarnecki, J. B., Simulated Effects of Increased Recharge on the Ground-Water Flow System of Yucca Mountain and Vicinity, Nevada-California, U. S. Geol. Surv. Water-Resources Investigations Report 84-4344, 1984.

Eakin, T. E. , G. B. Maxey, T. W. Robinson, J. C. Fredericks, and O. J. Loeltz, Contributions to the Hydrology of Eastern Nevada: Nevada Department of Conservation and Natural Resources Water Resources Bulletin 12,14-16, 1951.

Edelfsen, N. E., and A. B. C. Anderson, Thermodynamics of Soil Moisture, Hilgardia, 15(2), 31-298, 1943.

Environment Assessment Report, U. S. DOE report DOE/RW-0073, 1986.

Jackson, R. D., P. J. Pinter, Jr., R. J. Reginato, Net Radiation Calculated from Remote Multispectral and Ground Station Meteorological Data, Agric. Forest Meteorol., 35,153-164, 1985.

Kipp, K. L., Jr., Effect of Topography on Gas Flow in Unsaturated Fractured Rock-Numerical Simulation, Proc. Symp. Flow and Transport in Unsaturated Fractured Rock, AGU Geophysical monograph 42, edited by D. D. Evans and T. J. Nicholson, Am. Geophys. Union, Washington, DC, 171-176, 1987.

Klavetter, E. A., and R. R. Peters, Estimation of Hydrologic Properties of an Unsaturated Fractured Rock Mass, SAND84-2642, Sandia Nat. Lab., Albuquerque, N. M., 1986.

Lachenbruch, A. H., and Sass, J. H., Heat flow in the United States and the Thermal Regime of the Crust, in *The Earth's Crust--Its Nature and Physical Properties,* ed. by J. G. Heacock, Am. Geophys. Union Geophysical Monograph 20, 626-675, 1977.

Langkopf, B., Problem Definition Memo for COVE3a Benchmarking Problem, Sandia Nat. Lab., Albuquerque, NM, March 26, 1987.

Mandelbrot, B. B., *The Fractal Geometry of Nature,* W. H. Freeman, San Francisco, 1983.

Montazer, P. and W. E. Wilson, Conceptual Hydrological Model of Flow in the Unsaturated Zone, Yucca Mountain, Nevada, U. S. Geol. Surv. Water-Resources Investigations Report 84-4345, 1984.

Montazer, P., E. P. Weeks, F. Thamir, D. Hammermeister, S. N. Yard, and P. B. Hofrichter, Monitoring the Vadose Zone in Fractured Tuff, Ground Water Monitoring Review, 8(2), 72-88, 1988.

Peters R. R. and E. A. Klavetter, A Continuum Model for Water Movement in an Unsaturated Fractured Rock Mass, Water Resour. Res., 24(3), 416-430, 1988.

Pruess, K., Y. W. Tsang, and J. S. Y. Wang, Modeling of Strongly Heat Driven Flow in Partially Saturated Fractured Porous Media in Proc. IAH 17th International Congress on the Hydrogeology of Rocks of Low Permeability, 486-497, Univ. of Arizona, Tuscon, AZ, 1985.

Pruess, K., J. S. Y. Wang, and Y. W. Tsang, Effective Continuum Approximation for Modeling Fluid and Heat Flow in Fractured Porous Tuff, SAND 86-7000, Albuquerque, NM, 1988.

Quiring, R. F., Precipitation Climatology of the Nevada Test Site, National Oceanic and Atmospheric Administration, National Weather Service Report WSNSO 351-88, 1983.

Ross, B., A Conceptual Model of Deep Unsaturated Zones with Negligible Recharge, Water Resour. Res., 20, 11, 1627-1629, 1984.

Ross, B., Gas-phase Transport of Carbon-14 Released from Nuclear Waste into the Unsaturated Zone, paper presented in the 11th International Symposium on the Scientific Basis for Nuclear Waste Management, 1987.

Rush, F. G., Regional Ground-Water Systems in the Nevada Test Site Area, NYE, Lincoln, and Clark Counties, Nevada, Water Resources - Reconnaissance Series, Rep. 54, 1970.

Sass, J. H., and A. H. Lachenbruch, Preliminary Interpretation of Thermal Data from the Nevada Test Site, U. S. Geol. Surv. open-file report 82-973, 1982.

Stricker, H. and W. Brutsaert, Actual Evapotranspiration over a Summer Period in the "Hupsel Catchment", J. Hydrol. 39, 139-157, 1978.

Tsang, Y. W. and K. Pruess, A Study of Thermally Induced Convection Near a High-Level Nuclear Waste Repository in Partially Saturated Fractured Tuff, Water Resour. Res., 23 (10), 1958-1966, 1987.

Vargaftik, N. B., *Tables on the Thermophysical Properties of Liquids and Gases,* 2nd ed., John Wiley, NY, 1975.

Von Konynenburg, R. A., C. F. Smith, H. W. Culham, and C. H. Otto, Jr., Behavior of Carbon-14 in Waste Packages for Spent Fuel in a Repository in Tuff, in Scientific Basis for Nuclear Waste Management, vol. 8, ed. by C. M. Jantzen et al., Materials Research Society, Pittsburg, Pa., 405-412, 1985.

Von Konynenburg, R. A., C. F. Smith, H. W. Culham, and H. D. Smith, Carbon-14 in Waste Packages for Spent Fuel in a Tuff Repository, UCRL REP. 94708, Lawrence Livermore Nat. Lab., Livermore, CA, 1986.

Waddell, R. K., J. H. Robinson, and R. K. Blankennagel, Hydrology of Yucca Mountain and Vicinity, Nevada-California--Investigative results through mid 1983, U. S. Geog. Surv. Water Resources Investigations Report 84-4267, 1984.

Walker, W. R., J. D. Sabey, and D. R. Hampton, Studies of Heat Transfer and Water Migration in Soils, Final report, Department of Agricultural and Chemical Engineering, Colorado University, Fort Collins, CO, April 1981.

Weeks, E. P., Effect of Topography on Gas Flow in Unsaturated Rock-Concepts and Observations, Proc. Symp. Flow and Transport in Unsaturated Fractured Rock, AGU Geophysical monograph 42, edited by D. D. Evans and T. J. Nicholson, Am. Geophys. Union, Washington, DC, 165-170, 1987.

Weeks, E. P. and W. E. Wilson, Preliminary Evaluation of Hydrologic Properties of Cores of Unsaturated Tuff, Test Well USW H-1, Yucca Mountain, Nevada, U. S. Geol. Surv. Water Resources Investigations Report 84-4193, 1984.

Winograd, I. J., Radioactive Waste Disposal in Thick Unsaturated Zones, Science, 212(4502), 1457-1464, 1981.

Winograd, I. J., and W. Thordarson, Hydrologicic and Hydrochemical Framework, South-Central Great Basin, Nevada-California, With special reference to the Nevada Test Site: U. S. Geol. Surv. Professional Paper 712-c, 1975.

APPENDIX A
EFFECTIVE CONTINUUM CHARACTERISTICS CURVES

In the effective continuum, the suction pressure P_{suc}, and the equivalent continuum permeabilities to the liquid and gas phase, k_l and k_g, are expressed in terms of the continuum liquid saturation, S_l. When an effective continuum approximation is applicable, it is necesary to define the effective continuum parameters in terms of matrix and fracture parameters. The corresponding parameters for the fracture and matrix media will be denoted by subscript f and m respectively. The material properties and the characteristics curves for the fracture and matrix media are tabulated in Table 2.

(1) Threshold liquid saturation

Let S_l be the liquid saturation of the effective continuum. It is expressed in terms of the matrix and fracture saturations as follows (Pruess et al., 1988):

$$S_l = \frac{S_{lm}\phi_m + S_{lf}\phi_f}{\phi_m + \phi_f} \tag{A-1}$$

where both ϕ_m and ϕ_f are void fractions defined in terms of the total volume,

$$V_{tot} = V_m + V_f \,. \tag{A-2}$$

The threshold saturation, S_{th} is defined as the continuum liquid saturation at the juncture when the matrix is fully saturated and the fracture is dry, that is, S_{th} is the value of S_l in Equation (A-1) where S_{lm} is 1 and S_{lf} is 0,

$$S_{th} = \frac{\phi_m}{\phi_m + \phi_f} = .9839 \tag{A-3}$$

for the values of $\phi_m = .11$ and $\phi_f = .0018$ as tabulated in Table 2. The line of reasoning that leads to the definition of threshold liquid saturation is as follows. An effective continuum concept is only applicable when approximate local thermodynamic equilibrium exists between matrix and fractures. Because the capillary suction in the matrix is much stronger then that in the fracture, local equilibrium implies that the liquid saturation in the matrix will be much higher than that in the fracture. The threshold continuum saturation as defined by Equation (A-3) is based on the approximation that the enormous disparity of the strength of capillary suction in the matrix and fractures will cause the fractures to remain dry until the matrix becomes completely saturated.

From Equation (A-1), given the liquid saturation of the effective continuum, S_l, the matrix and fracture liquid saturation are as follows:

$$S_{lm} = S_l / S_{th}, \quad S_{lf} = 0; \qquad \text{for } S_l \le S_{th}$$

$$S_{lm} = 1, \quad S_{lf} = \frac{(S_l - S_{th})}{(1 - S_{th})}; \qquad \text{for } S_l > S_{th} \tag{A-4}$$

(2) Capillary suction

The capillary suction for the effective continuum in terms of the continuum saturation S_l is

$$P_{suc}(S_l) = P_{suc}(S_{lm} - \delta) \qquad \text{for } S_l < S_{th}$$
$$= P_{suc}(1-\delta) \cdot \frac{(1-S_l)}{(1-S_{th})} \qquad \text{for } S_l \geq S_{th} \qquad \text{(A-5)}$$

The matrix characteristic curve as tabulated in Table 2 is used for P_{suc}. The formulation in Equation (A-5) gives a continuous curve as the continuum liquid saturation passes through the threshold value. Below the threshold, it follows the suction curve for the matrix; above the threshold, the capillary suction in the fracture varies linearly with S_l. The parameter δ is introduced to represent air entry effects; i.e., a finite suction is required to reduce the matrix saturation from $S_{lm} = 1$. It gives the added advantage that the slope of dP_{suc}/dS_{lm} remains finite at S_{th}. The infinite slope of dP_{suc}/dS_{lm} at $S_{lm} = 1$ would have made the transition across the threshold impossible physically and numerically. A choice of δ corresponding to a suction pressure of a couple of thousands of Pascals (.2 m of H_2O) is sufficient to render the numerical computation possible. For the P_{suc} with parameters as tabulated in Table 2, this corresponds to a δ of $2x\ 10^{-6}$.

(3) Effective continuum liquid and gas permeability

The effective continuum liquid and gas permeabilities as fuctions of the effective continuum liquid saturation are defined in terms of the permeabilities in the matrix and fracture continua.

$$k_l(S_l) = \bar{k}_m(1-\phi_f)k_{rm}(S_{lm}) \qquad \text{for } S_l \leq S_{th}$$
$$= \bar{k}_m(1-\phi_f) + \bar{k}_f k_{rf}(S_{lf}) \qquad \text{for } S_l > S_{th} \qquad \text{(A-6)}$$

Equation (A-6) makes use of the fact that below S_{th}, the liquid saturation in the fracture continuum is 0 and therefore the relative permeability to the liquid in the fracture is zero; whereas above S_{th}, the matrix continuum is fully saturated with relative permeability equals 1. The $\bar{k}_m$ and $\bar{k}_f$ are respectively the saturated continuum permeabilities for the matrix and fracture, their values are given in Table 2. The effective continuum permeability to the gas may be expressed as the difference between the saturated permeability of the effective continuum and the permeability to the liquid phase, that is,

$$k_g(S_l) = [\bar{k}_m(1-\phi_f) + \bar{k}_f] - k_l(S_l). \qquad \text{(A-7)}$$

where the expression in the square bracket is the saturated permeability of the effective continuum.

We should point out here that the effective continuum concept for isothermal, single phase liquid flow has been developed by Peters and Klavetter (1988), who based their continuum model on the assumption of local pressure equilibrium between the matrix and fracture. The independent variable for their continuum characteristic curves is the suction pressure head; while we have used the liquid saturation as the independent variable in our derivation of the characteristic curves for two phase flow.

APPENDIX B

In this appendix we discuss the source of data used in this report, and when applicable, the values we used shall be compared to those used in RIB (Reference Information Base).

With reference to Problen specification in Table 2, which is divided in 3 sections: Material properties, Characteristic curves, and Binary diffusion parameters, only the first section has corresponding values in RIB. Reference source for each section is found on the right hand side of respective section heading in Table 2.

For the second section in Table 2 on characteristic curves, we used the Van Genuchten parameters given by Klavetter and Peters (1986). The parameters we adopted are those given for fracture and the matrix of Topopah Spring welded unit TSw 2. Our parameter λ in Table 2 is related to β as tabulated in Klavetter and Peters (1986) by $\lambda = 1 - 1/\beta$; and our value of 1.7562 MPa for suction pressure in matrix is based on the conversion $\rho g(1/\alpha)$ where α is expressed in m^{-1} in Klavetter and Peters (1986). We used the density of water $\rho(20\,^{\circ}C) = 998.2\,kg/m^3$ for the conversion.

Binary diffusion parameters in the third section of Table 2 are not available in RIB. Langkopf (1987) suggested the values for D^{o}_{va} and θ from Bird et al. (1960). We chose the tortuosity factor of $\tau = 1$ and porosity, ϕ, that of the fracture based on the reasoning that the gas phase flow predominantly takes place in the fractures.

The values in the first section of table 2 are identical to those given in Tsang and Pruess (1987) and Pruess et al. (1988). In the latter, a RIB appendix exists where the values we used were related to those in RIB version 1.001. When we commenced the calculations in this report, we consulted RIB version 2.001. In the following Tabulation, we shall compare our values with the latest RIB version 4.001.

Appendix B						
Parameter	Author's Value	RIB Value		RIB Ver 4.000		Remarks
		mean	standard deviation	Subsection	Page	
Rock density	$\rho = 2580 kg/m^3$	$2.55 g/cm^3$	.032	1.2.1,	p. 3	Value used within RIB range for TSw 2
Rock specific heat	$C_R = 840 J/kg\ C$	Thermal capacitance ($J/cm^3\ K$) of the rock mass at 25 C 1.9779 for TSw 1 2.0324 for TSw 2 1.8443 for TSw 3		1.2.4,	p. 3	Using our matrix porosity of 0.11 and rock grain density of 2580 kg/m^3, we get for thermal capacitance: $C_R(1-\phi_m)\rho_R = 1.92\ J/cm^3\ K$
Matrix continuum permeability	$\bar{K}_m = 1.9 \times 10^{-18} m^2$	$1.9 \times 10^{-11} m/s$ (conversion: $1\ m/s \approx 10^{-7} m^2$)	N/A	1.4.3,	p. 6	Value in RIB is for vertical hydraulic conductivity for well UE-25b
Fracture continuum permeability	$\bar{K}_f = 1.8 \times 10^{-14} m^2$	N/A		--	--	Our value is of the same order of magnitude as air permeability measurements in welded tuff (Montazer et al., 1988)
Formation heat conductivity	1.74 W/m C (dry) 2.34 W/m C (wet)	2.23 W/m C	.047	1.2.2,	p. 3	RIB value for TSw 2
Matrix porosity	$\phi_m = .11$	.121	.036	1.2.1,	p. 3	RIB Value for TSw 2
Fracture porosity	$\phi_f = .0018$	N/A		--	--	RIB version 2.001, 1.1.4.3, p. 3 gives .0028; p. 4 gives .00018
Surface Temperature	T = 12.85 C	54.9 F (12.7 C)		1.5.1,	p. 2	RIB value is for average annual temperature for Yucca Flat
Temperature at 600 m depth	T = 30.85 C	--	--	--	--	Derived from surface temperature coupled with typical thermal gradient of .03 C/m. RIB 1.2.7, p. 3, gives temperature profile in well USW G-4, T at 600m depth ~ 31 C

Table 1.
Representative values of suction pressure, P_{cap} at 286 K corresponding to lower relative humidity, h.

h	$P_{cap} = \ln h\ (\rho_l RT)$
0.9	-1.3906×10^7 Pa
0.8	-2.9451×10^7 Pa
0.7	-4.7075×10^7 Pa
0.5	-9.1483×10^7 Pa
0.3	-1.5890×10^8 Pa
0.2	-2.1242×10^8 Pa

Table 2.
Problem Specification

Material Properties	(RIB)
rock grain density	$\rho_R = 2580\ kg/m^3$
rock specific heat	$C_R = 840\ J/kg°C$
matrix continuum permeability (at fully saturated condition)	$\bar{k}_m = 1.9 \times 10^{-18}\ m^2$
fracture continuum permeability (at fully saturated condition)	$\bar{k}_f = 1.8 \times 10^{-14}\ m^2$
formation heat conductivity (dry)	$K_{Dry} = 1.74\ W/m\ °C$
formation heat conductivity (at liquid saturation S_l)	$K = K_{Dry} + .6\ S_l$
matrix porosity	$\phi_m = .11$
fracture porosity	$\phi_f = .0018$
Characteristic Curves	**Klavetter and Peters, 1986**
relative permeability to liquid for matrix	$k_{rm}(S_{lm}) = \sqrt{S_{EF}}\,(1-(1-S_{EF}^{\frac{1}{\lambda}})^{\lambda})^2$ $S_{EF} = \frac{S_{lm} - S_{lr}}{1 - S_{lr}}$ $S_{lr} = .0801, \lambda = .4438$
relative permeability to liquid for fracture	$k_{rf}(S_{lf}) = \sqrt{S_{EF}}\,(1-(1-S_{EF}^{\frac{1}{\lambda}})^{\lambda})^2$ $S_{EF} = \frac{S_{lf} - S_{lr}}{1 - S_{lr}}$ $S_{lr} = .0395, \lambda = .76359$
suction pressure for matrix	$P_{suc}(S_l) = P_{suc}(S_{lm})$ $= -1.7265\,(S_{EF}^{-1/\lambda} - 1)^{1-\lambda}$ MPa (matrix values used for S_{EF}, λ)
Binary Diffusion Parameters	**(Bird et al., 1960; Langkopf, 1987)**

$D^{\circ}_{va} = 2.14 \times 10^{-5}\ m^2/sec$

$\theta = 2.334$

$\tau = 1$

$\phi = \phi_f$

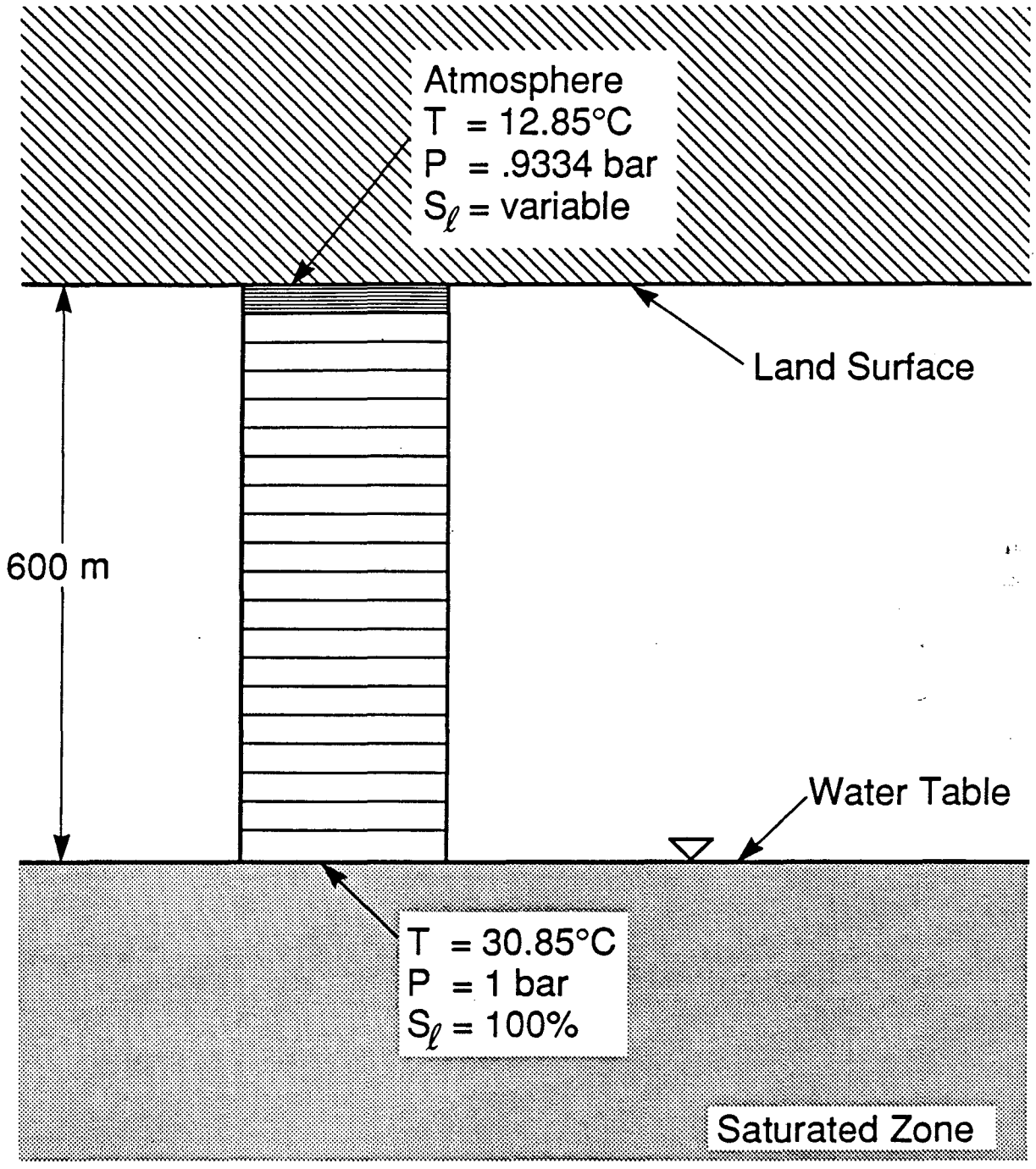

XBL 882-10033

Figure 1 One-dimensional vertical column for simulation studies of humidity effects at the land surface.

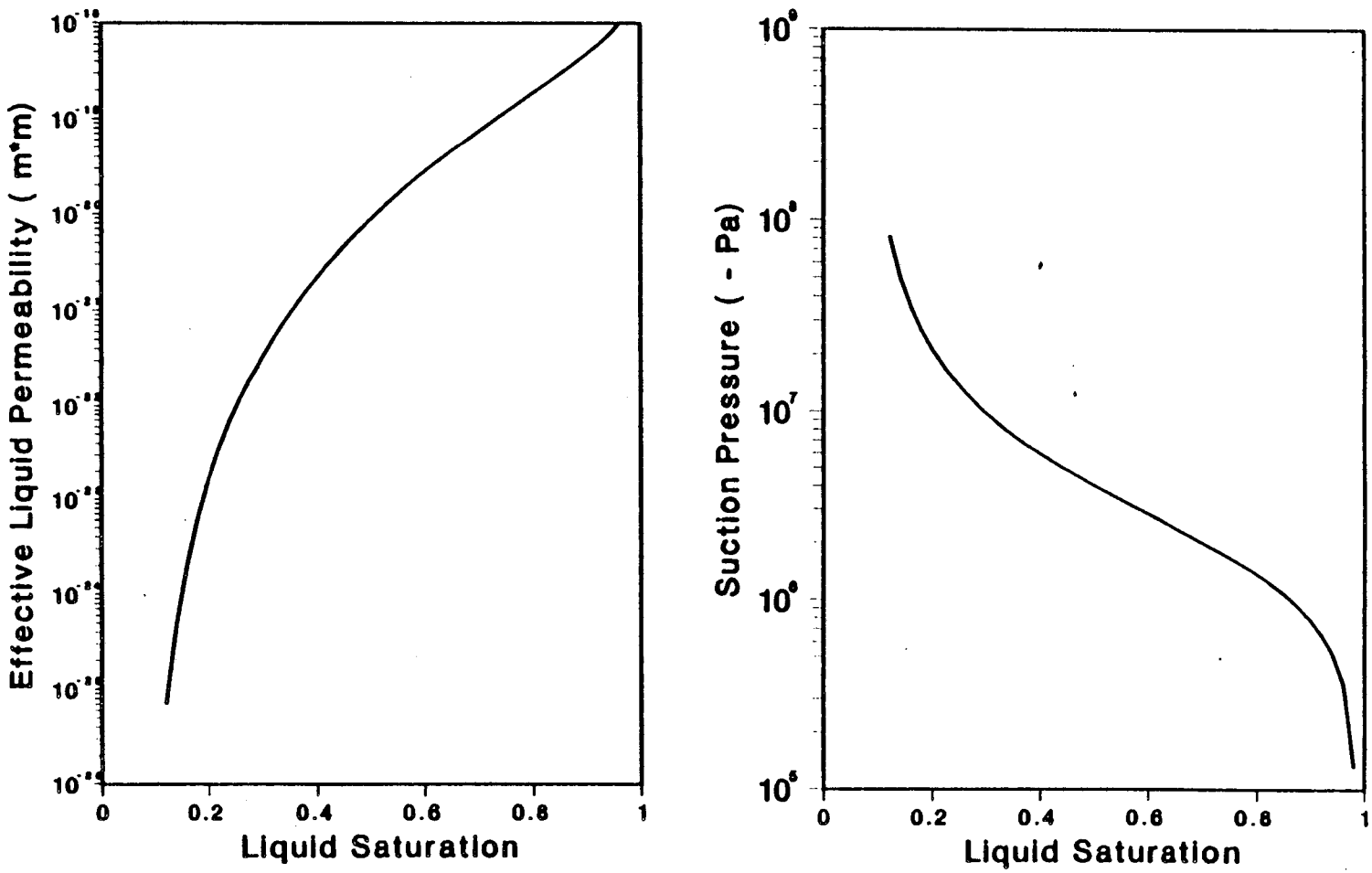

Figure 2 The characteristic curves for the fractured porous medium (Topopah Spring welded unit): (a) the effective liquid permeability, (b) the capillary suction pressure.

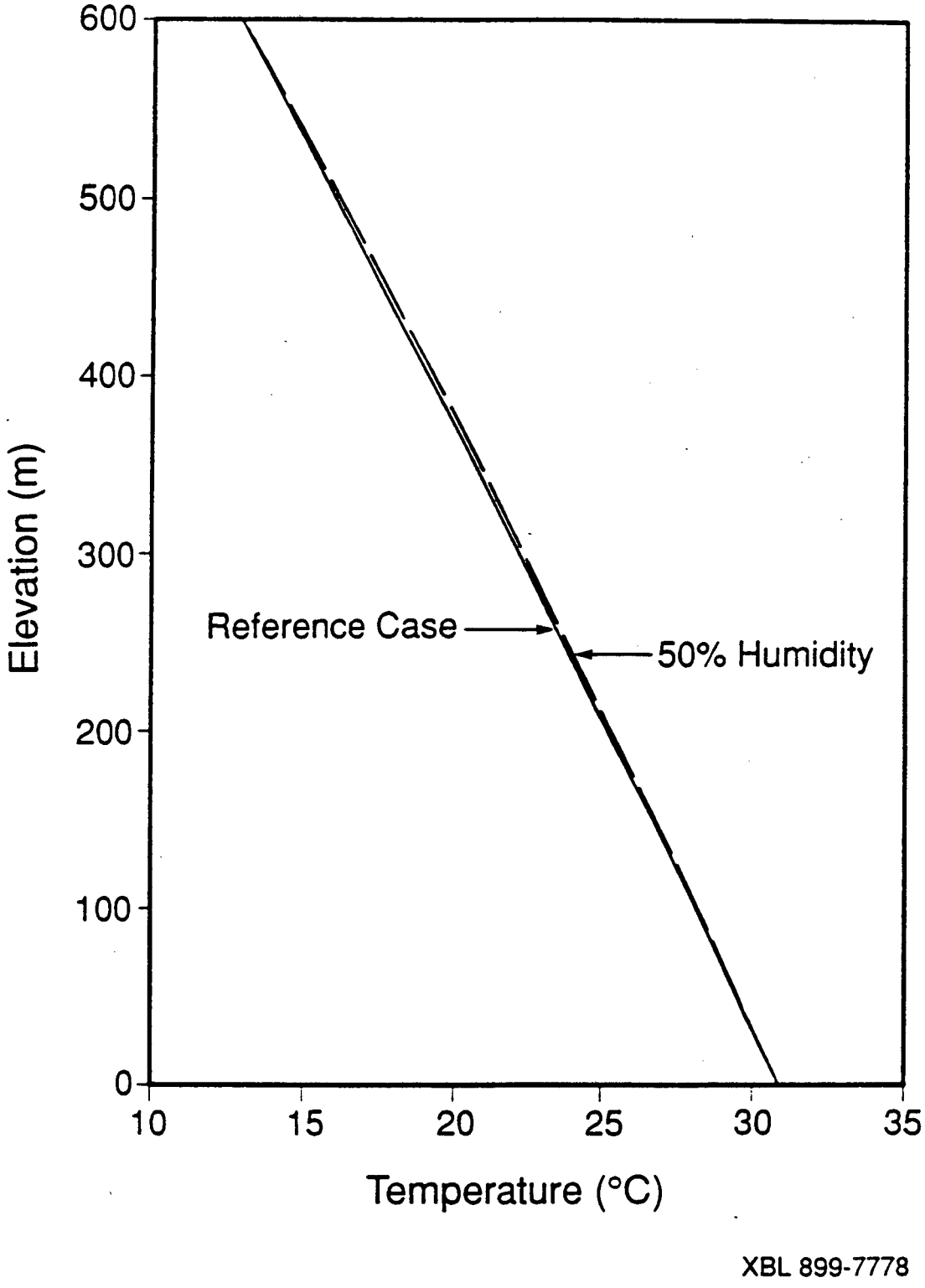

Figure 3 The temperature variation with elevation (with reference to water table) for ambient conditions and humidity boundary conditions at land surface.

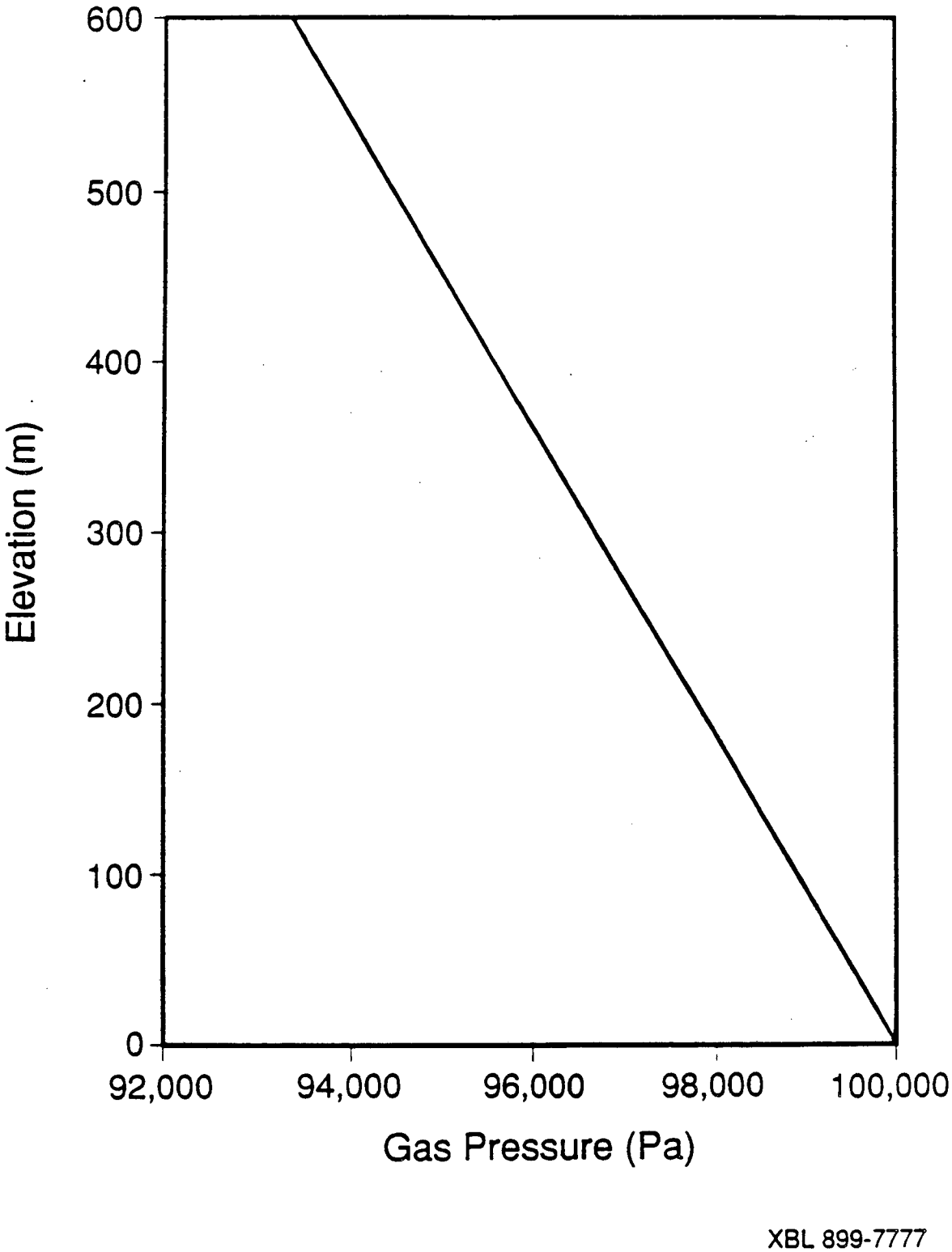

Figure 4 Equilibrium gas pressure profile with elevation for ambient conditions.

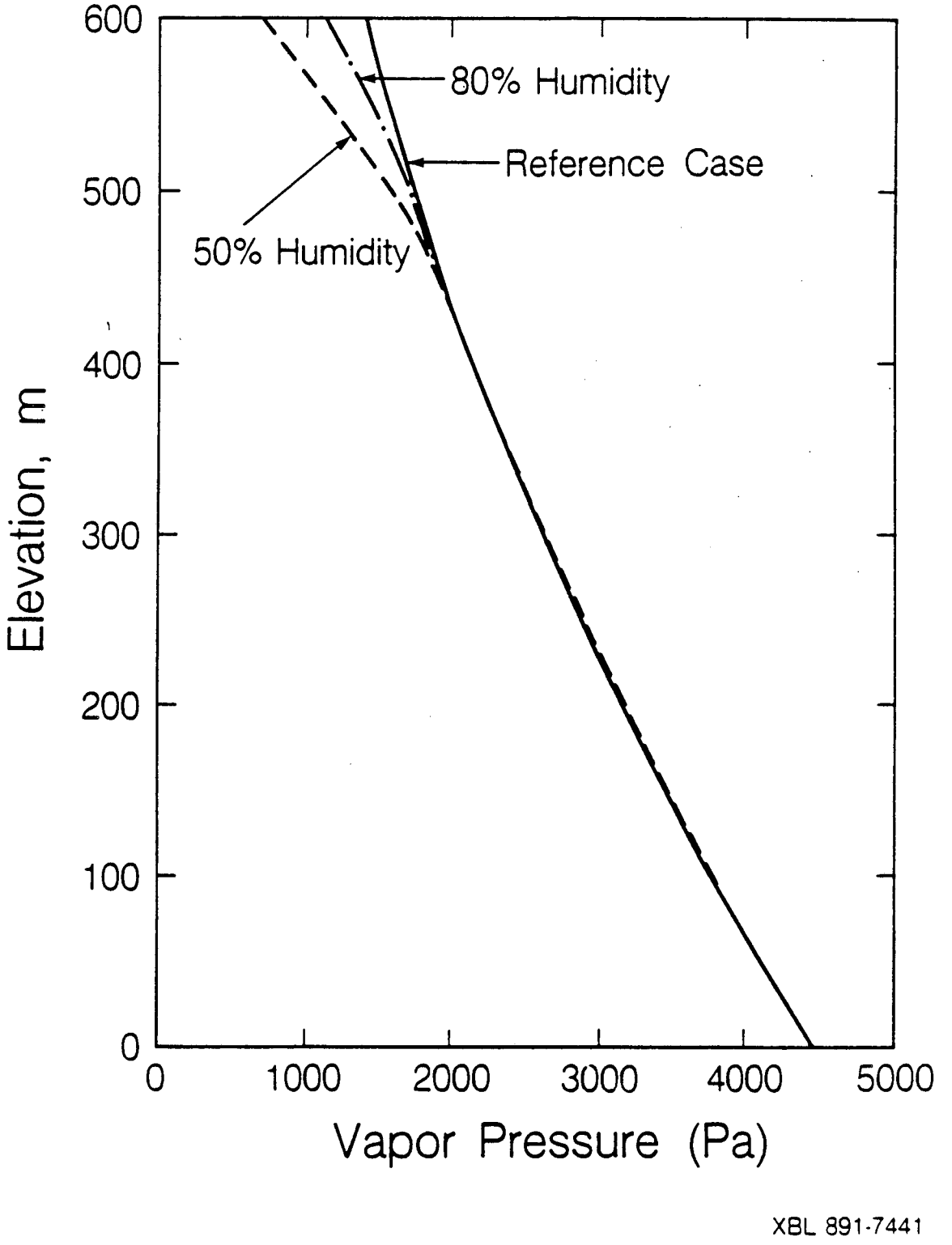

Figure 5 Vapor pressure profiles for ambient conditions and humidity boundary conditions.

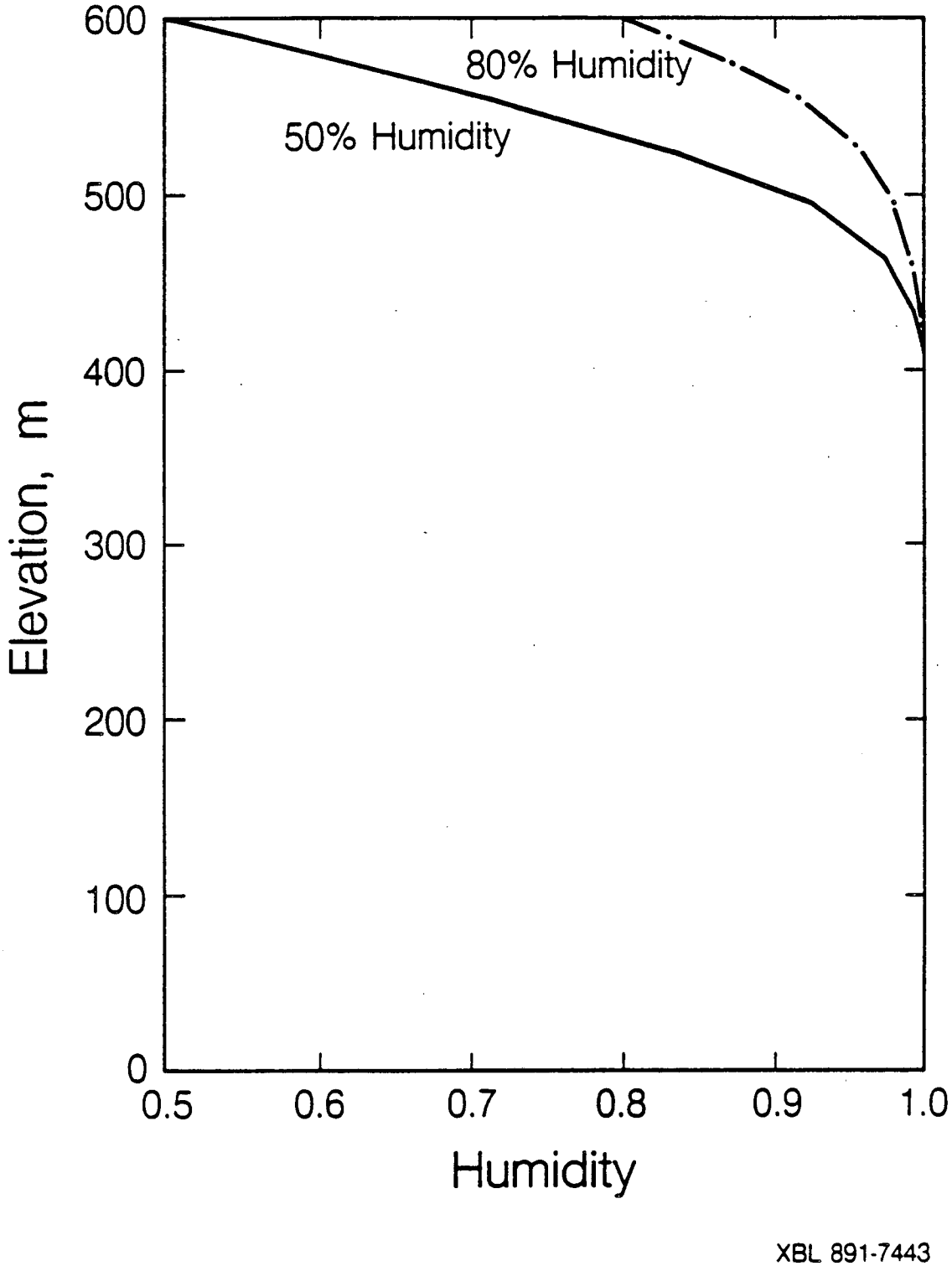

Figure 6 Profiles of relative humidity of soil gas for ambient conditions and humidity boundary conditions.

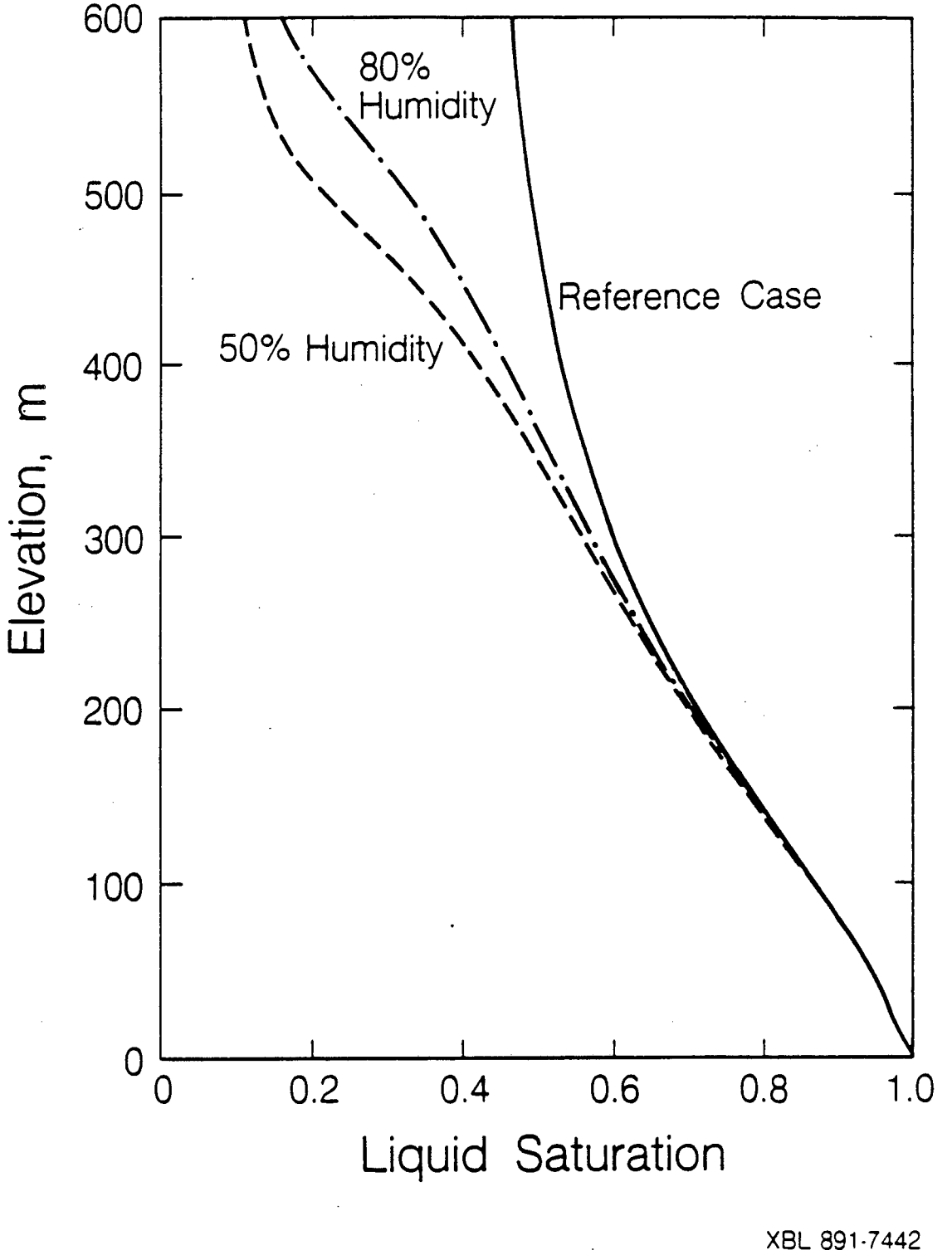

Figure 7 Liquid saturation profiles for ambient conditions and humidity boundary conditions.

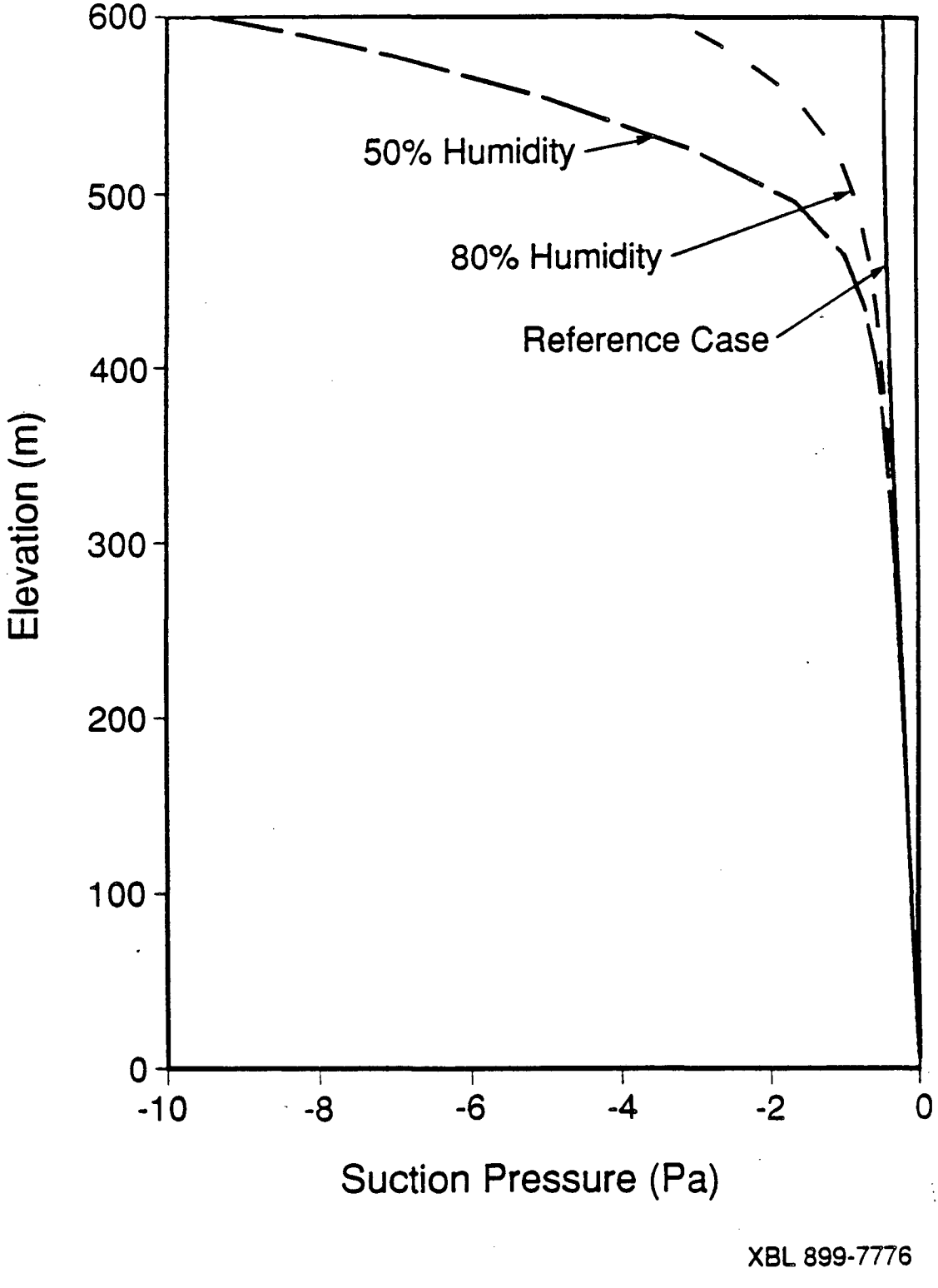

Figure 8 Capillary suction pressure profiles for ambient conditions and humidity boundary conditions.

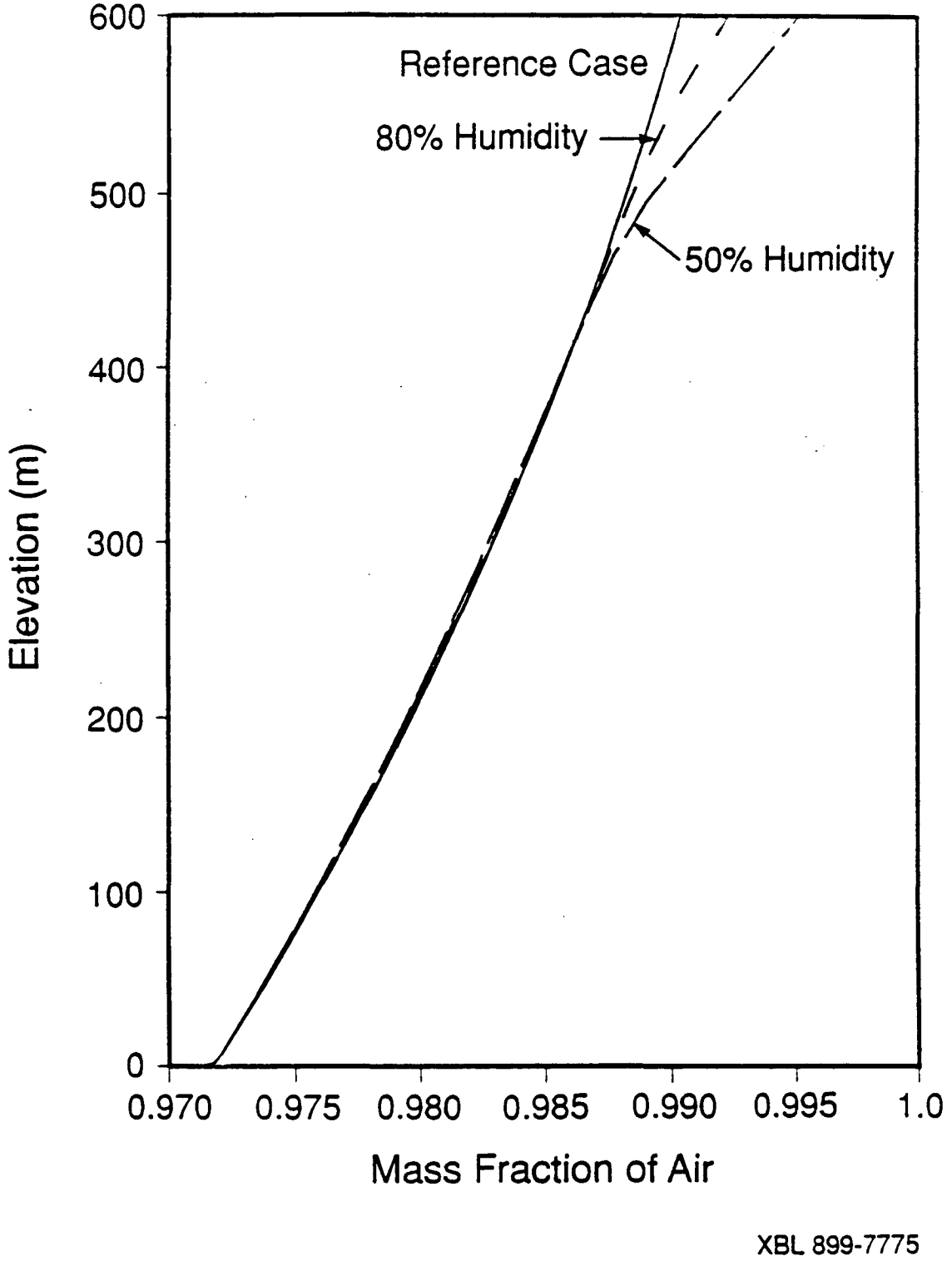

Figure 9 Profiles of mass fraction of air in the gas phase for ambient conditions and humidity boundary conditions.

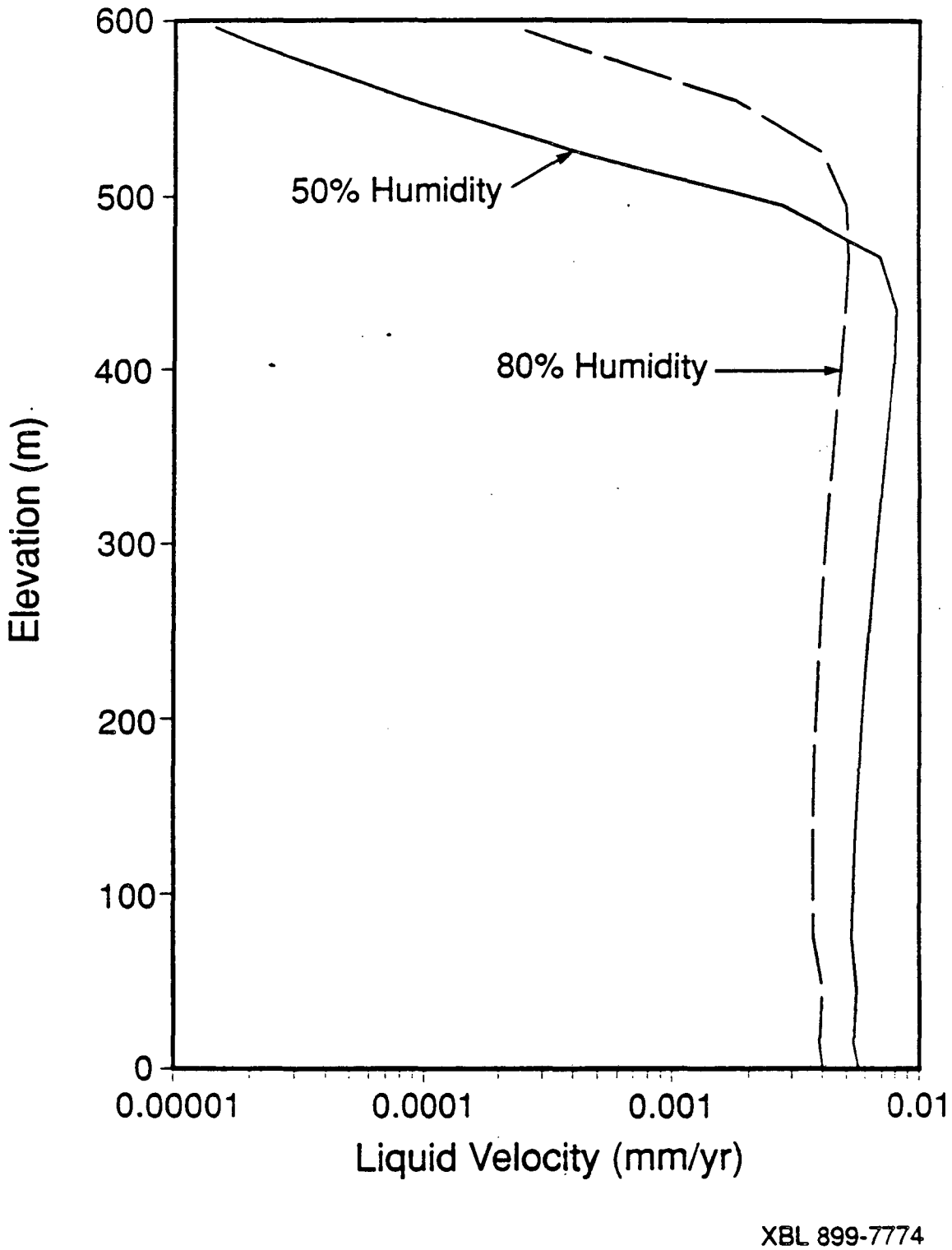

Figure 10 Profiles of upward liquid Darcy velocity with humidity boundary condition.

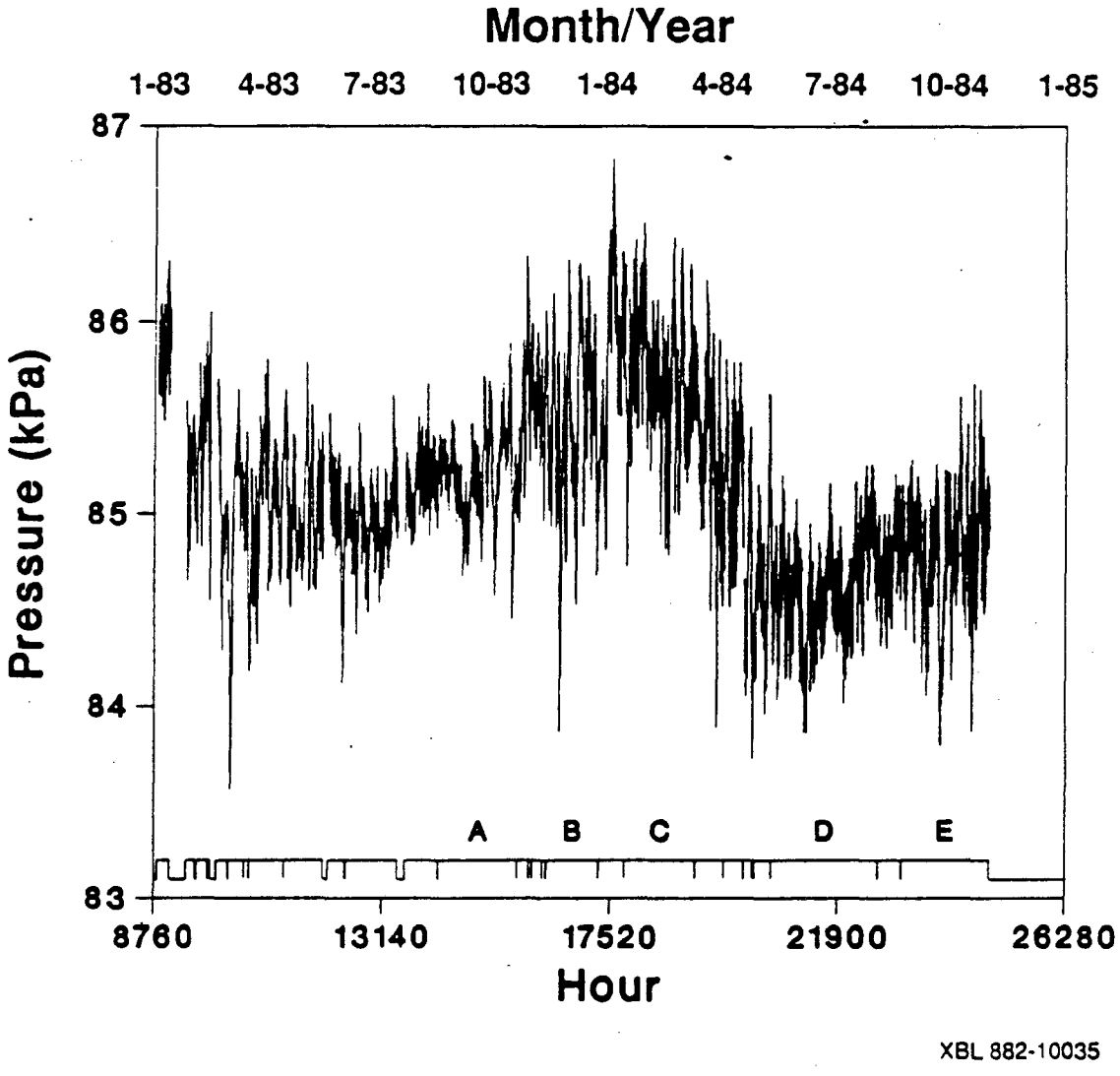

Figure 11 Hourly atmospheric pressure data at Yucca Ridge over a 2 year period.

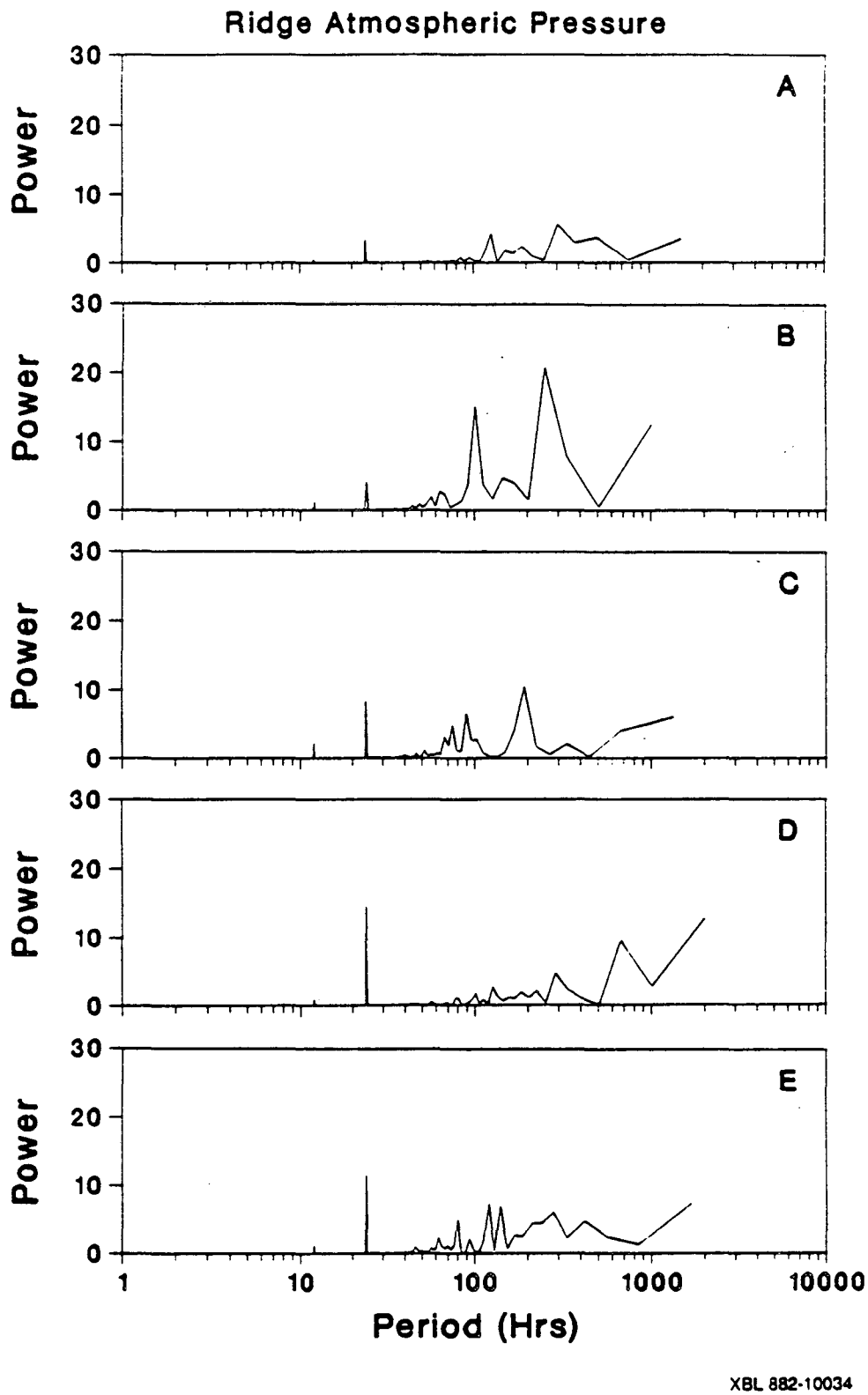

Figure 12 Fourier power spectrum derived from short segments of pressure data in Figure 11 (segments A - E, each of 2-3 months duration).

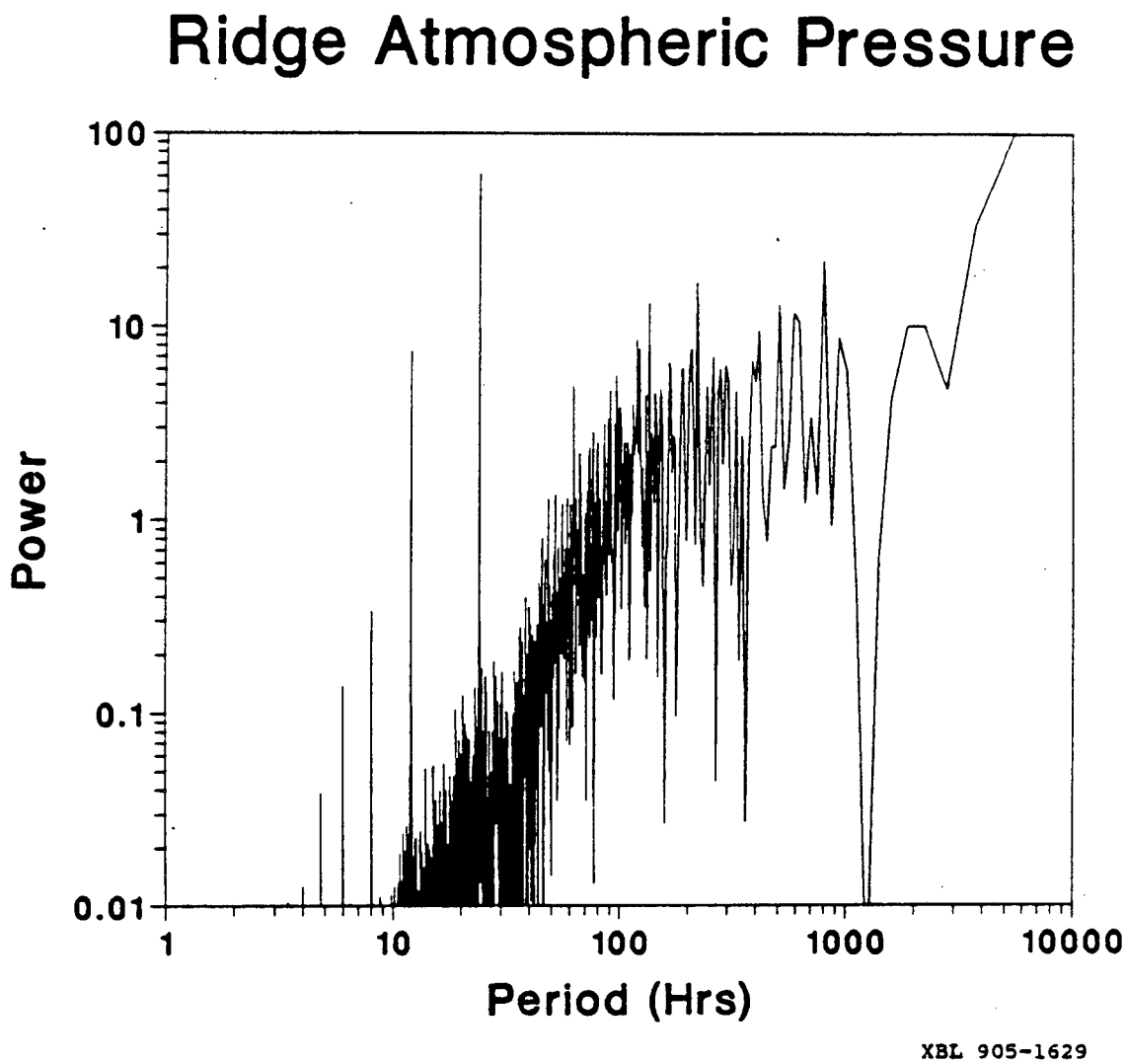

Figure 13 Fourier power spectrum derived from pressure data in Figure 11 covering about 15 months.

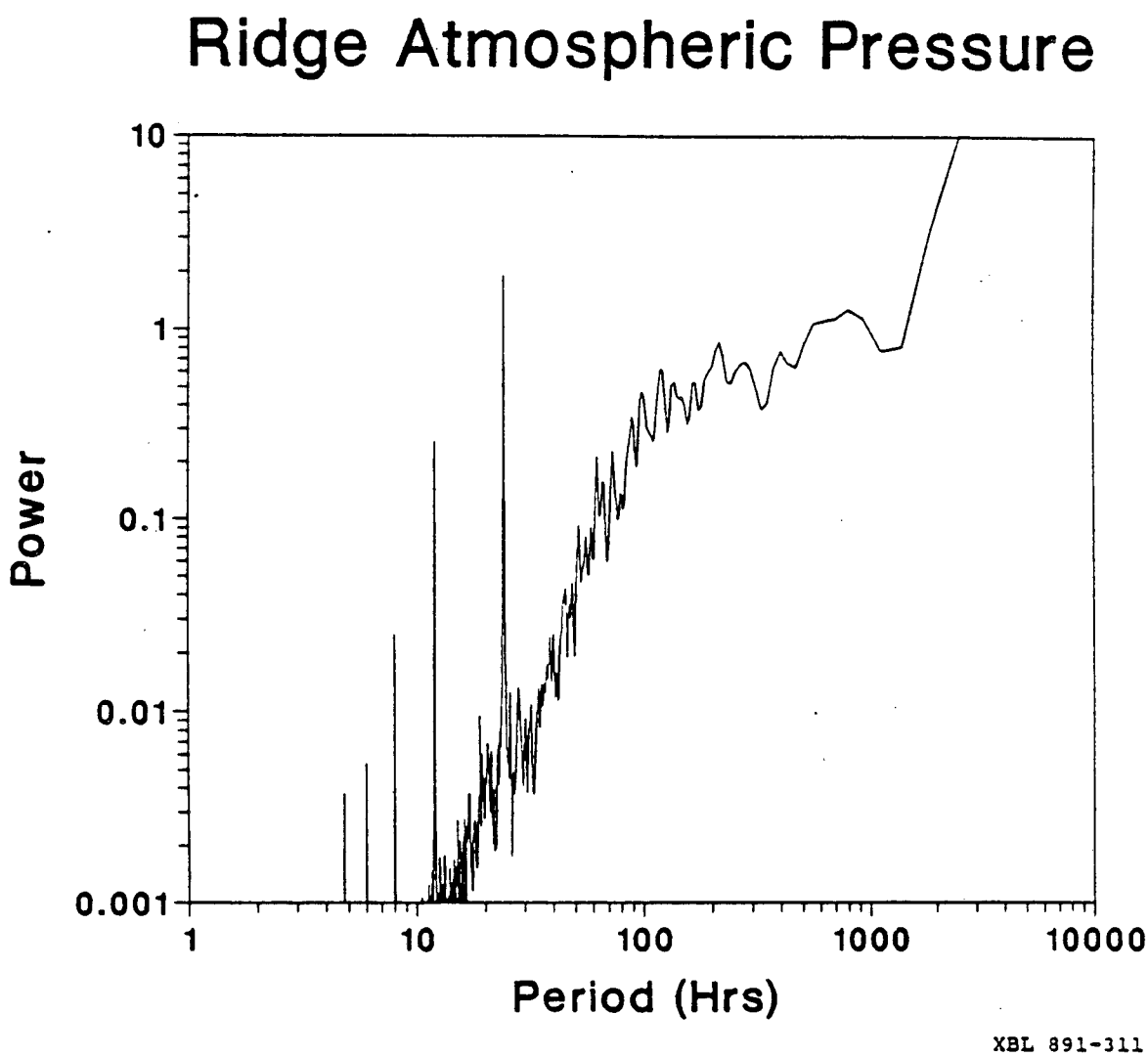

Figure 14 Smoothed Fourier power spectrum of atmospheric pressure data.

LAWRENCE BERKELEY LABORATORY
UNIVERSITY OF CALIFORNIA
INFORMATION RESOURCES DEPARTMENT
BERKELEY, CALIFORNIA 94720